Area-Selective Deposition to Enable Single-digit nm Fabrication

2019 CNF REU Intern: James M.H Tran

2019 CNF REU Intern Affiliation:
Electrical Engineering, The University of Texas at Dallas

CNF Project: 2019 Cornell NanoScale Science & Technology Facility Research Experiences for Undergraduates Program

CNF REU Principal Investigator(s): Prof. James R. Engstrom, Chemical and Biomolecular Engineering, Cornell University

CNF REU Mentor(s): Taewon Suh and Colleen C. Lawlor, Chemical and Biomolecular Engineering, Cornell University

Primary Source of CNF REU Funding: National Science Foundation via the National Nanotechnology Coordinated Infrastructure (NNCI) Grant No. NNCI-1542081

Contact: tranj@utdallas.edu, jre7@cornell.edu, ts695@cornell.edu, ccl233@cornell.edu

Website: http://cnf.cornell.edu/education/reu/2019

Primary CNF Tools Used: Photolithography spinners and hot plates, GCA AS200 stepper, Oxford 81/82 (80+) RIE etchers, Anatech resist strip, CVC SC4500 e-beam evaporator (odd), Logitech Orbis CMP

Abstract:

As semiconductor manufacturing approaches single-digit nm feature sizes, there is an increasing difficulty in reliably patterning critical device features. A major obstacle is that conventional top-down techniques suffer from issues with alignment of device features during the manufacturing process. Area-selective deposition (ASD) seeks to remedy this by a bottom-up technique; selectively depositing films only on defined growth areas and not on non-growth regions, creating a "self-aligned" feature. We produce line and space patterned wafers of metal and dielectric, copper and silicon dioxide in this study, to serve as a substrate for ASD experiments. We use various characterization techniques, such as optical microscopy and scanning electron microscopy (SEM), to evaluate our wafers. We also discuss intended uses of these wafers in ASD experiments.

Introduction:

For decades, top-down manufacturing has been the method of choice for fabricating semiconductor devices. However, as we approach single-digit nm feature sizes, device patterning becomes problematic. At this scale, pattern misalignment can severely affect device functionality and operation. This misalignment is known as the "edge placement error" [1], which is defined as the distance between the actual and intended position of a patterned feature. ASD could achieve device patterning at the single-digit nm scale by utilizing a bottom-up approach, selectively depositing thin films using atomic layer deposition (ALD) or chemical vapor deposition (CVD) on defined deposition areas. By depositing thin films only on intended areas, any possibility of misalignment could be eliminated, because a "self-aligned" feature is created. In addition to resolving feature misalignment, ASD also introduces advantages such as uniform, conformal, and Angstrom level thickness controlled deposition of thin films.

In this study, 10, 5, 3, and 1 μm line and space patterns of Cu and SiO_2 were fabricated to study ASD of thin films. Alternating metal and dielectric patterns allow investigation of ASD of thin films on Cu and not on SiO_2, or vice versa. Variable widths of Cu and SiO_2 enable study of how film growth varies with different feature sizes. The pattern also has equal line and space widths of Cu and SiO_2, producing a 50/50 area coverage of metal and dielectric for *in situ* x-ray photoelectron spectroscopy (XPS) studies.

Experiment Details:

500 nm SiO_2 on 100 mm Si wafers were utilized. Wafers were cleaned in a Hamatech automated wafer processer with piranha solution before spin coating. Brewer Science WiDE-C 15C bottom anti-reflective coating (BARC) was spun at 3000 RPM for 60 seconds before a two-step bake on a 190°C proximity hotplate for 60 seconds, followed by a 160°C vacuum hotplate for 60 seconds. OiR 620-7i photoresist was spun at 5000 RPM for 60 seconds followed by a pre-exposure 90°C vacuum hotplate bake for 60 seconds. Exposure was performed on a GCA AS200 stepper, followed by a post-exposure bake on a 115°C vacuum hotplate. Etching was performed using the Oxford 80+ reactive ion etcher. BARC was etched using an O_2 and Ar mixture for six minutes. SiO_2 was etched with a mixture of CHF_3 and Ar for 6:30 minutes to etch ~ 220 nm into the SiO_2. Resist and BARC were stripped using an Anatech O_2 plasma dry strip, followed by a piranha clean. A CVC SC4500 e-beam evaporator was then used to deposit 25 nm of Ta as an adhesion layer, followed by

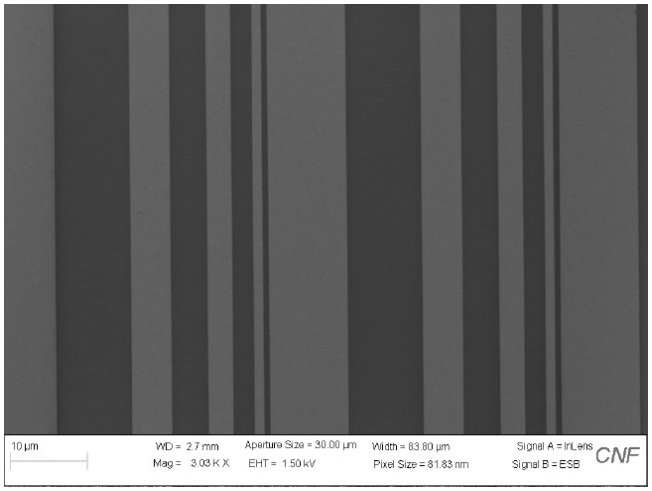

Figure 1: Top-down optical microscope image of 10, 5, 3, and 1 µm widths of Cu and SiO_2. Bright areas correspond to Cu and dark blue to SiO_2.

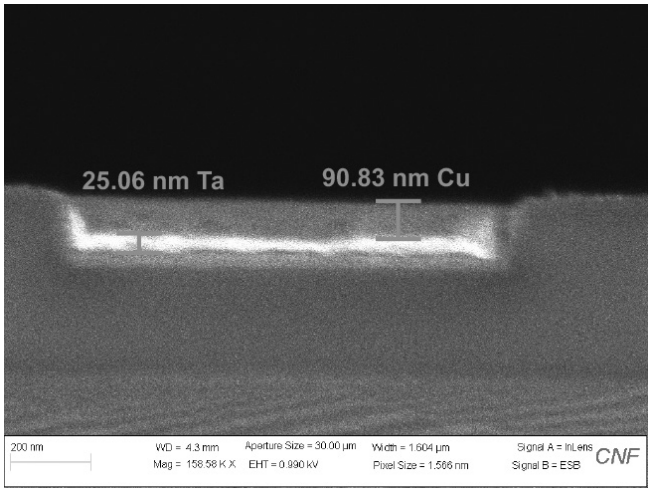

Figure 2: Cross-sectional SEM image of a 1 µm width trench filled with 90.83 nm Cu on top of 25.06 nm Ta.

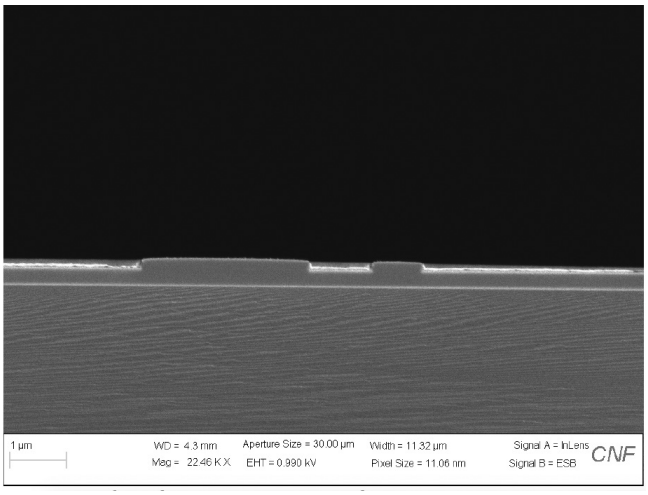

Figure 3: Etch uniformity across varying feature sizes.

300 nm Cu. Logitech-Orbis CMP was finally used to planarize the surface and remove Cu overburden at 4 psi down and 30 psi back pressure for 1:50 minutes. A Hamatech was then used again to clean the wafer of CMP debris.

Results and Discussion:

Optical microscope images showed a definite line and space pattern of Cu and SiO_2. Images confirm enough Cu overburden was polished away to reveal the desired pattern, as shown in Figure 1. Cross-sectional SEM images show the anisotropic etch profile, and the Cu and Ta layers deposited in Figure 2. Ta was deposited as an adhesion layer between the Cu and the SiO_2. Without Ta, Cu would rip out of the trenches during the CMP step due to its poor adhesion to SiO_2. No metal was seen on top of the SiO_2, and the Cu line was level with the SiO_2 space. Etch depth and anisotropic profile was consistent across varying feature sizes, as shown in Figure 4. The depth of Cu was kept greater than 70 nm, thick enough to serve as a substrate layer for surface-sensitive analysis techniques such as XPS. CHF_3 and Ar was chosen as the etch chemistry for its anisotropic etch profile. The gas mixture combines physical etching from Ar and chemical etching from CHF_3. CHF_3 provides F radicals that etch SiO_2 [2,3]. Ar^+ ions etch the SiO_2 by breaking its crystal bonds. Ar^+ also desorbs the fluoropolymer film generated by the CHF_3 radicals, exposing horizontal surfaces to the etch gases [2]. The fluoropolymer keeps the etch directional, by passivating the sidewalls of the SiO_2 preventing lateral etching.

Conclusions:

We successfully developed a robust and reproducible process to fabricate patterned line and space wafers. The ability to perform experiments on a patterned wafer will greatly enhance our understanding of area selective deposition.

Acknowledgements:

Thanks to ERG and CNF staff for insight and helpful discussion. This work was performed in part at the Cornell NanoScale Facility via the 2019 CNF REU Program. The CNF is a member of the National Nanotechnology Coordinated Infrastructure (NNCI), which is supported by the National Science Foundation (Grant NNCI-1542081).

References:

[1] Mackus, A.J.M., M.J.M. Merkx, and W.M.M. Kessels. "From the Bottom-Up: Toward Area-Selective Atomic Layer Deposition with High Selectivity." Chemistry of Materials 31, no. 1: 2-12. https://doi.org/10.1021/acs.chemmater.8b03454 (January 8, 2019).

[2] Fuller, Lynn, "Plasma Etching", Microelectronic Engineering, Rochester Institute of Technology.

[3] Kunimasa Takahashi, et al. 1994 Jpn. J. Appl. Phys. 33 4745.

Metal-Organic Hybrid Photoresists

CNF Project Number: 386-90
Principal Investigator(s): Christopher Kemper Ober
User(s): Kazunori Sakai, Seok-Hyon Jung, Wenyang Pan

Affiliation(s): Materials Science and Engineering, Cornell University
Primary Source(s) of Research Funding: JSR Corporation
Contact: christoper.ober@cornell.edu, ks2288@cornell.edu, sj736@cornell.edu, wp222@cornell.edu
Primary CNF Tools Used: Zeiss Supra SEM, ASML 300C DUV stepper, ABM contact aligner

Abstract:

While extreme ultraviolet (EUV) lithography is being investigated for patterning under 20 nm half pitch pattern size, further improvement is needed for achieving high volume manufacturing. EUV lithography uses a wavelength of 13.5 nm and this brings about the biggest problem of EUV lithography that a typical EUV power source is incapable of generating enough photons compared to other light sources. In this circumstance, materials enabling use of fewer EUV photons have been investigated. In this report, microscale patterning results of metal-organic cluster resists with high EUV absorption composition and EUV exposure results of zinc organic cluster resist on different underlayer are described.

Summary of Research:

While continuous effort has been dedicated to the extreme ultraviolet (EUV) lithography to follow Moore's law, further improvement is needed for achieving high volume manufacture.

One of the reasons why manufacturing by EUV lithography has taken a longer time to develop than other lithography techniques is typical EUV sources provide fewer numbers of photons than other light sources. In terms of materials, photoresists including higher EUV absorption and better underlayer materials absorbing EUV transmitted through the photoresist and assisting additional generation of acid have been investigated. Inorganic elements possess higher EUV absorption than organic elements and EUV photoresist, including metal oxide nanoparticles or metal complexes have been attracting interest.

We developed hafnium and zirconium oxide nanoparticle resist and have recently focused on developing zinc-organic cluster resist with controlled molecular weight and size distribution [1].

In this report, the lithography performance of other metal-organic cluster resists and the effect of underlayer for EUV lithography performance are discussed. The micro-scale patterning results are shown in Figure 1.

Transition metals such as Group 4 metals, cobalt and nickel and non-transition metals such as indium and tin are available. Especially, cobalt and nickel are expected to absorb more EUV light, and further study will be investigated.

The EUV exposure results of zinc-organic cluster resist on the different underlayer are summarized in Figure 2. The introduction of underlayer has improved the sensitivity with the almost same LWR value. The mechanism based on this phenomenon will be elucidated.

References:

[1] Xu, H., Sakai, K., Kasahara, K., Yang, K., Herbol, H. C., Odent, J., Clancy, P., Giannelis, E. P., Ober, C. K., Metal-Organic Framework-inspired metal-containing building units for high resolution patterning, Chem. Mater. 2018, 30, 4124-4133.

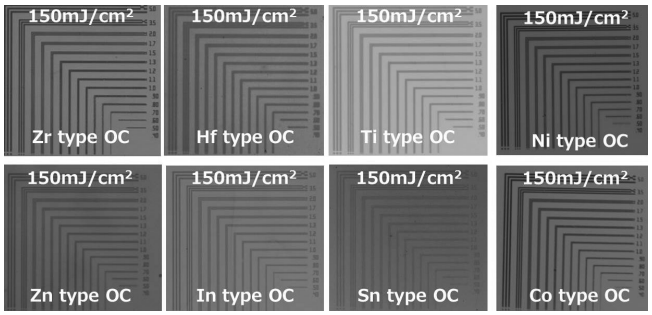

Figure 1: Optical microscope images of micro-scale patterning using the ABM contact aligner.

Resist	Sample-A	Sample-A	Sample-A	Sample-A
Substrate	Bare-Si	UL-A	UL-B	UL-C
Image @16nmLS	67mJ/cm2 LWR 5.0nm	58mJ/cm2 LWR 5.2nm	51mJ/cm2 LWR 5.6nm	54mJ/cm2 LWR 5.2nm

Figure 2: SEMs of EUV exposure results with zinc organic cluster resists.

Transient Laser Heating Derived Mesoporous Materials Directed by Gyroidal Templates from Block Copolymer Self-Assembly

CNF Project Number: 1356-05

Principal Investigator(s): Ulrich Wiesner

User(s): Qi Zhang, Fei Yu

Affiliation(s): Department of Materials Science and Engineering, Cornell University

Primary Source(s) of Research Funding: National Science Foundation (DMR-1719875)

Contact: ubw1@cornell.edu, qz224@cornell.edu, fy84@cornell.edu

Website: http://wiesner.mse.cornell.edu/

Primary CNF Tools Used: TFT N+/P+ Polysilicon Furnace - A4, Oxford 81 etcher

Abstract:

Equilibrium thin-film gyroidal carbon was fabricated from co-assembly of an amphiphilic triblock terpolymer and resorcinol-formaldehyde resols through solvent vapor annealing. Upon crosslinking the resols and carbonizing the thin films, mesoporous carbon templates were obtained. Low-pressure chemical vapor deposition (LPCVD) was utilized to deposit amorphous silicon into the templates. Pulsed excimer laser irradiation melted and crystallized the deposited silicon through a non-equilibrium nanosecond-scale process that preserves the underlying organic template. Finally, after removing the carbon template, we successfully prepared 3D continuous crystalline silicon with the inverse gyroidal nanostructure.

Summary of Research:

Templates enable the manufacturing of objects with intricate and complicated structures. Templates at the nanoscale allow for fabrication of nanomaterials that could find applications in catalysis or microelectronics. Block copolymer self-assembly offers bottom-up pathways to complex nanostructured templates, which can be combined with laser annealing for pattern transfer to produce porous ordered nanomaterials after template removal.

We first prepared such nanoscale organic templates derived from block copolymer in co-assembly with carbon precursors. To this end, poly(isoprene)-*block*-poly(styrene)-*block*-poly(ethylene oxide) (PI-*b*-PS-*b*-PEO, or ISO) was synthesized via sequential anionic polymerization as described elsewhere [1]. The resorcinol-formaldehyde resols, i.e. the carbon precursors, are hydrogen bonded to the PEO block of the amphiphilic ISO terpolymer. Through solvent vapor annealing, the resols were structure-directed by ISO and they formed an equilibrium co-continuous structure known as alternating gyroids on silicon wafers [2]. After the resols were crosslinked and carbonized at high temperatures, mesoporous carbon thin-film templates with gyroidal nanostructures were prepared (Figure 1).

These thin films derived from organic precursors are stable and amenable to nanomaterials fabrication and processing techniques, a prerequisite for any structure-directing template. We used LPCVD in the A4 Polysilicon Furnace at CNF to backfill the mesopores with undoped Si (Figure 2). Following TFT MOS cleaning procedures, the native oxide layer between the carbon templates and silicon wafers was removed by dipping them in diluted 20:1 hydrofluoric acid (HF) without compromising the ordered mesostructure of the organic templates. The resulting thin films have small grains of silicon filling the pores with a silicon overlayer on top.

In order to achieve conformal backfilling with crystalline materials, carbon templates with amorphous silicon deposited were subject to pulsed laser annealing at ambient atmosphere. Previous research [3] has demonstrated that shortening heating times promotes the thermal stability of organic materials. Transient excimer laser irradiation for 40 ns delivered enough energy to melt the silicon (melting temperature around 1250°C). The resulting crystallized silicon displayed polycrystallinity, with the carbon template remaining intact after the heating process.

A combination of dry and wet etching was utilized to remove the carbon template from the carbon/silicon hybrid. Using the Oxford 81 etcher at CNF, reactive ion etching was carried out with CF_4 and oxygen, and brief dipping in HF exposed the carbon template to the outside.

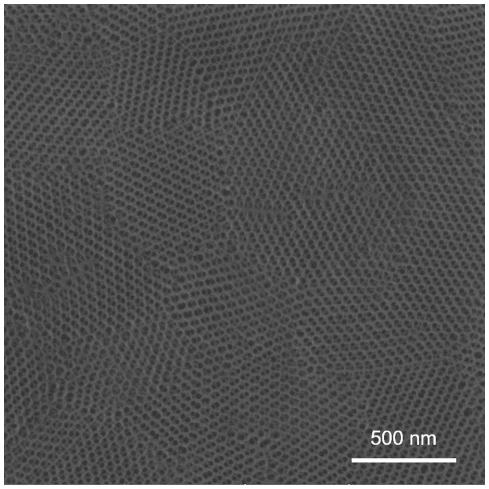

Figure 1: Scanning electron microscopy (SEM) plan view of the mesoporous gyroidal carbon template, derived from ISO-resols hybrid carbonized at 450°C.

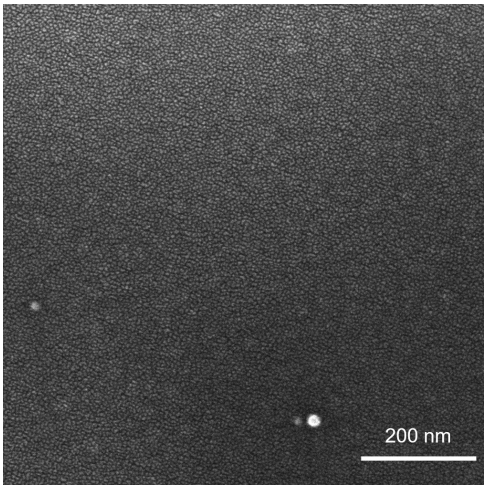

Figure 2: SEM plan view of the carbon template with Si deposited through LPCVD. There is a Si overlayer on top of the template, showing grains of silicon.

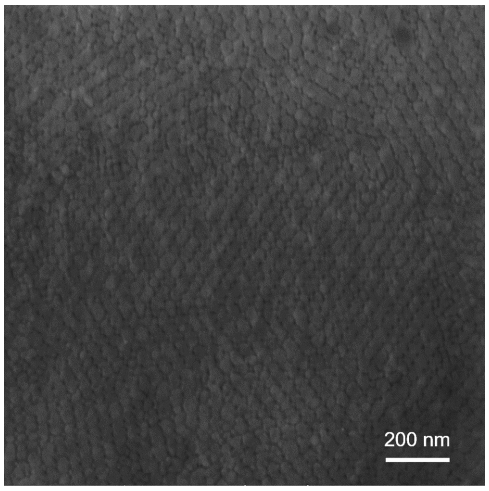

Figure 3: SEM plan view of crystalline silicon nanostructures after template removal, leaving behind interconnected trenches.

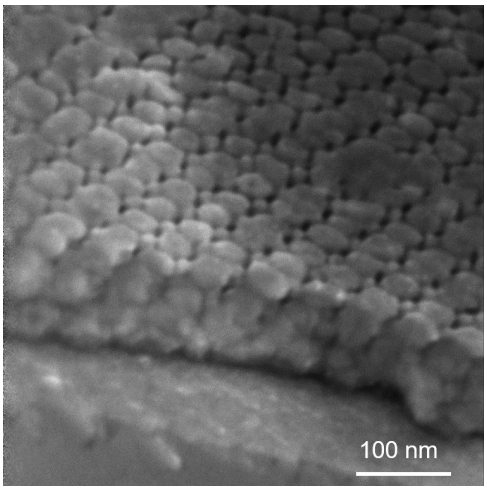

Figure 4: SEM cross-section view of crystalline silicon nanostructures after template removal, leaving behind interconnected trenches.

We subsequently immersed the samples in piranha solution at elevated temperatures to decompose the carbon template. The 3D continuity of gyroids ensures complete removal of the template. Periodically ordered crystalline silicon with the inverse nanostructure of the carbon template was finally obtained via brief dipping in HF to remove silicon oxide (Figures 3 and 4).

Our fabrication route makes compatible the processing of organic soft materials and inorganic semiconductors and capitalizes on the highly non-equilibrium nature of transient laser heating. This same strategy can be expanded to other materials, such as metals and compound semiconductors, to be backfilled into the template.

The resulting mesoporous crystalline materials could allow us to explore interesting functionalities in areas including sensing, catalysis, and microelectronics.

References:

[1] Bailey, T. S. et al. A Noncubic Triply Periodic Network Morphology in Poly (Isoprene-b-Styrene-b- Ethylene Oxide) Triblock Copolymers. Macromolecules 35, 7007-7017 (2002).

[2] Zhang, Q. et al. Pathways to Mesoporous Resin/Carbon Thin Films with Alternating Gyroid Morphology. ACS Nano 12, 347-358 (2018).

[3] Jung, B. et al. Kinetic Rates of Thermal Transformations and Diffusion in Polymer Systems Measured during Sub-millisecond Laser-Induced Heating. ACS Nano 6, 5830-5836 (2012).

Three-Dimensional Printing with Silica Cages

CNF Project Number: 1645-08

Principal Investigator(s): Tobias Hanrath

User(s): Jen-Yu Huang

Affiliation(s): Robert F. Smith School of Chemical and Biomolecular Engineering, Cornell University

Primary Source(s) of Research Funding: National Science Foundation

Contact: th358@cornell.edu, jh2486@cornell.edu

Primary CNF Tools Used: SEMs (Supra and Ultra), Leica supercritical dryer, AFM

Abstract:

Material scientists have now developed an extensive library of nano-sized building blocks, offering a vast panel of properties (optic, magnetic, plasmonic, catalytic, etc.). Nevertheless, combining these building blocks for the realization of multifunctional materials while controlling their structure from the nano- to the micro-and all the way to the macroscale still remains an open challenge in order to fully exploit their potential. In parallel, new material processing techniques such as 3D printing technologies are emerging for the fabrication of macroscopic highly engineered parts and devices. In this work, newly discovered silica nanocages are combined with digital light processing 3D printing technique for the rapid fabrication of mesoporous parts with arbitrary shapes and tunable internal structures. Complementary strategies are then deployed for the implementation and deliberate positioning of various functionalities throughout 3D printed objects with high control on the microstructure and macroscopic architecture of the superstructures. This approach paves the road for innovative device concepts and designs, that will benefit from the unique properties of nanomaterials and from the micro-and macroscale manufacturing capability of 3D printers.

Summary of Research:

In this work, the silica cages were made compatible with digital light processing 3D printing, through their functionalization with methyl methacrylate groups (Figure 1). In a previous study, calculations suggested that as part of their formation mechanism, the cages vertices and struts deform the surface of the micelles, with positively charged surfactant molecules wrapping the negatively charged inner surface of the cages. As illustrated in the inset of Figure 1a, this soft-template approach allows to distinguish the inner and outer surfaces of the cages, forcing the functional group to attach predominantly on the outer surface. Later in the synthesis process, the surfactant micelles were removed from the inside of the cages by dialysis in an acidic ethanol solution, causing the cages to precipitate in aqueous solution.

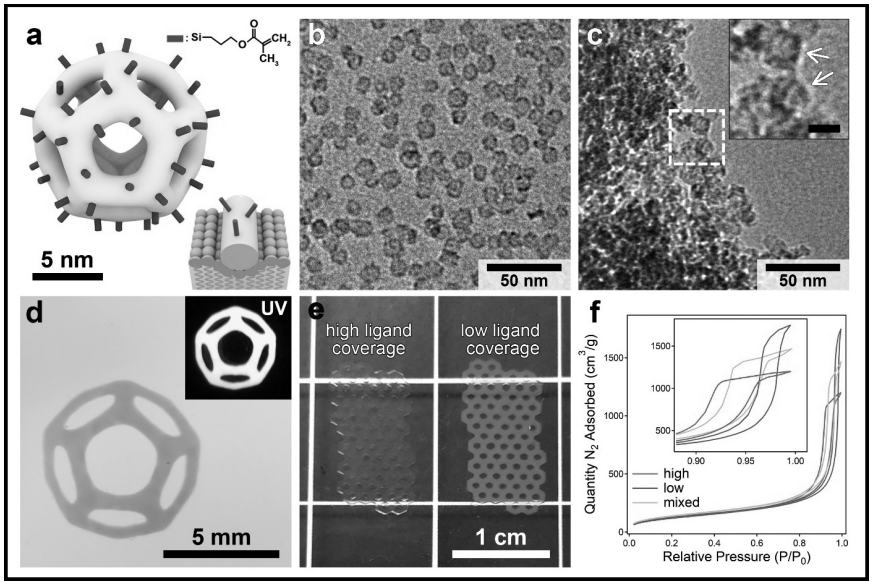

Figure 1: Illustration (a) and TEM image (b) of silica cages functionalized with methyl methacrylate groups (inset in a: illustration of a cage strut before removal of the surfactant micelle, in blue). (c) TEM image of a piece of a printed part (inset: zoom in, white arrows point to clearly visible cage structures, scale bar 10 nm). (d) Photography of a pattern printed on a glass substrate with dye functionalized cages (inset: photography under UV irradiation). (e) Photography of parts printed with silica cages with high (left) and low (right) methyl methacrylate surface coverage. (f) Nitrogen sorption isotherms of parts printed with high and low methyl methacrylate coverage, and with mixed samples (inset: zoom in the hysteresis range). (Find full color on pages xiv-xv.)

Although the original silica cage synthesis was upscaled 30 times in order to make the printing of large parts affordable, the transmission electron microscope (TEM) image in Figure 1b shows that cage structures were obtained with this modified method.

In Figure 1e, larger and free-standing parts exhibiting a honeycomb structure were printed with different ligand coverages and dried with Leica critical point dryer in CNF. For the part with low ligand coverage, the cages were functionalized with 2.5 times less than for the high ligand coverage. Although these two parts have the same dimensions, the low coverage one is 1.7 times lighter than the high coverage one. This important difference in density suggests different internal microstructures. These parts have relatively similar specific surface area, specifically 438 m^2g^{-1} and 450 m^2g^{-1} for the high and low coverage parts respectively, as determined by the Brunauer-Emmett-Teller (BET) method. Nevertheless, the hysteresis of the nitrogen sorption measurements (Figure 1f) show important difference in adsorption-desorption behavior.

The broader hysteresis of the high coverage part suggests that mesopores access is more restricted in this case, whereas in the low coverage part the mesopores access is facilitated by the presence of large pores and channels. This is also supported by the direct visual inspection of these parts (Figure 1e). While the high coverage part appears relatively transparent, the low coverage one is more translucent due to light scattering by larger pores. To induce significant Mie scattering, these larger pores should be at least few tens of nanometers in size and can only correspond to interparticle pores because the intraparticle pores, i.e. core of the cages, are less than 10 nm. Since the parts have similar specific surface area regardless of the ligand coverage, these large interparticle pores do not contribute significantly to the total surface area.

Instead, this property mostly derives from the intra-particle pores of the cage structures and from the microporosity of silica itself. Thus, varying the ligand coverage of cage-based PLIC inks is a powerful tool to purposefully tune the porosity and internal structure of 3D printed objects. Additionally, a PLIC ink was prepared by mixing the two cage samples in equivalent proportion. The isotherms of the resulting printed part, denoted as 'mixed' (Figure 1f), shows an intermediate behavior between those obtained with either purely high or low coverage, hence offering an additional knob to tune the microstructure of these macroscopic objects.

As an interesting feature, these parts can also be calcined in order to remove the organic component, yet fully preserving their fine microstructure.

Fabricating Advanced Characterization Platforms for Polyelectrolyte Brushes

CNF Project Number: 1757-09

Principal Investigator(s): Christopher Kemper Ober

User(s): Nilay Duzen

Affiliation(s): Materials Science and Engineering, Cornell University

Primary Source(s) of Research Funding: National Science Foundation

Contact: cko3@cornell.edu, nd387@cornell.edu

Primary CNF Tools Used: ASML 300C DUV stepper, SC4500 evaporator, Oxford PlasmaLab 80+ etch system, ZEISS SEM, Oxford ALD FlexAL, Unaxis 770 deep silicon etcher, Veeco Icon AFM

Abstract:

Polyelectrolyte brushes are a special class of polymer brushes with charges present along the backbone. They have unique properties and promising applications as stimuli responsive smart surfaces for numerous areas [1]. However, a greater fundamental understanding of the behavior and stability of these brush systems in different environments is still needed. Advanced characterization tools such as neutron scattering are helpful for this purpose. Here we report the development of a novel platform that has been used in neutron scattering studies of polyelectrolyte brushes. This design enabled the growth of brushes laterally from sidewalls of trenches of patterned silica surfaces and helped us to gain insight on the relationship between the backbone and charged group on polyelectrolyte brushes.

Summary of Research:

We employed a top-down process starting with patterning a silicon wafer. In order to prevent polymer brush growth from the top and bottom of the trenches, we decided to cover those parts with chromium film (about 5 nm thickness). However, since we don't want to have chromium residue on the sidewalls, we first deposited a sacrificial SiO_2 layer on the grating with atomic layer deposition (ALD). Then this layer is selectively removed from only the top and bottom of the trenches by reactive ion etching (RIE) followed by the deposition of chromium layers on these flat surfaces with atomic layer deposition. Potential chromium residue on the sidewalls is removed by hydrofluoric acid, which results in the desired grating design where the flat surfaces are covered with chromium to prevent polymerization, whereas sidewalls are covered with SiO_2 to be ready for lateral brush growth. Figure 1 summarizes the fabrication process.

After finishing the fabrication, poly(dimethyl amino-ethylmethacrylate) (PDMAEMA) brushes with different thickness were grown from the sidewalls of the grating. Since the top of the brushes do not feel steric repulsion due to the lack of confinement [2], the polymer chain stretching is the highest at the bottom of the grating and thickness decreases towards the top.

A schematic of the platform design with the polymer brush is shown in Figure 2. The neutron scattering studies that have been done with the help of our collaborators at the University of Sheffield showed good fit between the model and experimental specular data. Using these fits as input, we will further investigate brush profile by using off-specular data.

We are also planning to use the Cornell NanoScale Science and Technology Facility (CNF) for our new polyelectrolyte brush architecture that incorporates well defined charged side groups via peptoid structures. We are studying these brushes to see the effect of charge type and proximity to the backbone on brush behavior. We will use nanopatterning through CNF as a tool for controlling the geometric confinement and we will continue to fabricate the advanced platforms for further characterization of these new brush types.

References:

[1] Macromolecules 2017, 50 (11), 4089-4113.

[2] Macromolecules 2017, 50 (12), 4715-4724.

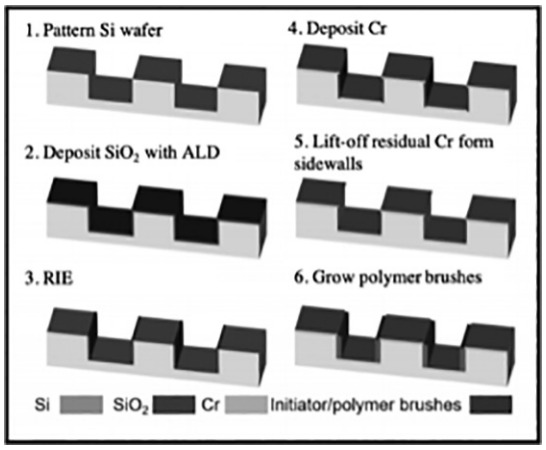

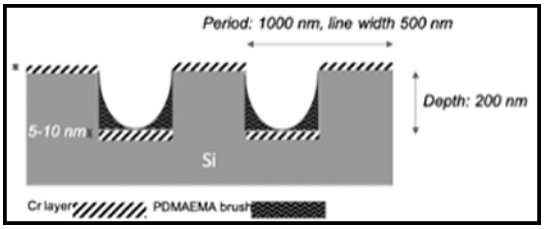

Figure 1,left: Fabrication process for advanced characterization platform.

Figure 2, above: Design details schematic of the platform showing polymer brush growth form sidewalls.

Nanometer-Scale Area-Selective Formation of Polymer Brushes

CNF Project Number: 1757-09

Principal Investigator(s): Christopher Kemper Ober[2]

User(s): Yuming Huang[2], Hai Quang Tran[1,2]

Affiliation(s): 1. School of Chemical and Biomolecular Engineering,
2. Department of Materials Science and Engineering; Cornell University

Primary Source(s) of Research Funding: National Science Foundation

Contact: cko3@cornell.edu, yh839@cornell.edu

Website: http://cober.mse.cornell.edu/index.html

Primary CNF Tools Used: E-beam resist spinners, JEOL 9500, FilMetrics F50-EXR, Oxford 81 etcher, Zeiss Ultra SEM, optical microscope

Abstract:

The topological control of polymer brushes can be realized via surface-initiated polymerization on a pattern fabricated by electron-beam (e-beam) lithography, which is known for its fine resolution and precision. Patterned polymer brushes were produced on silicon wafers by selective deposition of initiator, using patterned e-beam resists as the masks. As a result, cone-like polymer brushes with a height of ~ 60 nm and diameter of ~ 60 nm were formed in the desired pattern. This platform has several potential uses, including cytoskeleton mimicry and molecular recognition.

Summary of Research:

Introduction. Polymer brushes have a unique molecular structure with one end of the polymer chain covalently bonded to a substrate, such as a silicon wafer. Fabricating these brushes has been one of the main areas of focus in polymer science in recent decades and has demonstrated interesting applications in many fields [1]. The precise, nanometer-scale patterning of e-beam lithography can be incorporated with surface-initiated polymerization to provide a novel pathway in the area-selective placement of polymer brushes on hard substrates. This results in surfaces with anisotropic properties, unique chemical functionality, and responsive behavior under different stimulations.

Fabrication. The polymer brushes were patterned on a silicon wafer by depositing polymerization initiators selectively on desired areas. This was accomplished by patterning the e-beam resist (~150nm) through JEOL 9500 and using it as the mask for deposition. Before depositing the initiator, the surface of the substrate was etched ~ 10 nm to remove residual debris. The deposition of a silane initiator was carried out in the vapor phase, followed by the removal of the resist. Subsequently, surface-initiated ring-opening polymerization was carried out under vacuum and elevated temperature [2]. A schematic illustration of the fabrication process is shown in Figure 1.

Characterization and Results. The thickness of the e-beam resist was found using FilMetrics F50-EXR after spin-coating. After the exposure and developing process, the e-beam resist was analyzed by Zeiss Ultra SEM (Figure 2). The patterned polymer brushes were characterized using atomic force microscopy (AFM) in Cornell Center for Materials Research (Figure 3) for height measurement, and Zeiss Ultra scanning electron microscope (SEM) for topological analysis (Figure 4).

Conclusions. We demonstrated that e-beam lithography can be used to precisely control the spatial arrangement of polymer brushes. In the near future, we plan to explore the use of these surfaces for biological applications, such as cell membrane support and molecular recognition.

References:

[1] Chen, W.-L.; Cordero, R.; Tran, H.; Ober, C. K. 50th Anniversary Perspective: Polymer Brushes: Novel Surfaces for Future Materials. Macromolecules 2017, 50 (11), 4089-4113.

[2] Wang, Y.; Chang, Y. C. Preparation of Unidirectional End-Grafted α-Helical Polypeptides by Solvent Quenching. J. Am. Chem. Soc. 2003, 125 (21), 6376-6377.

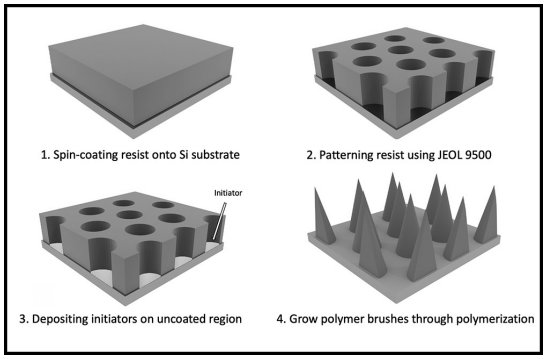

Figure 1: Schematic illustration of the fabrication process.

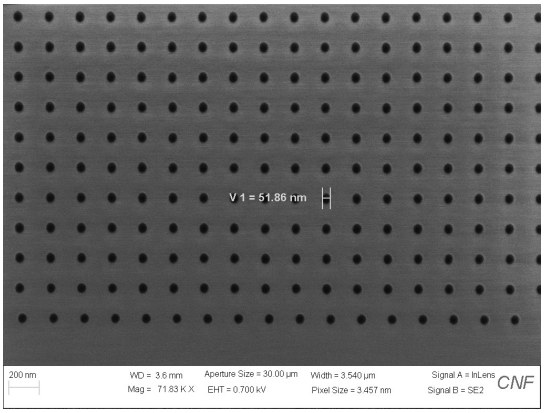

Figure 2: The e-beam pattern after the exposure and developing processes.

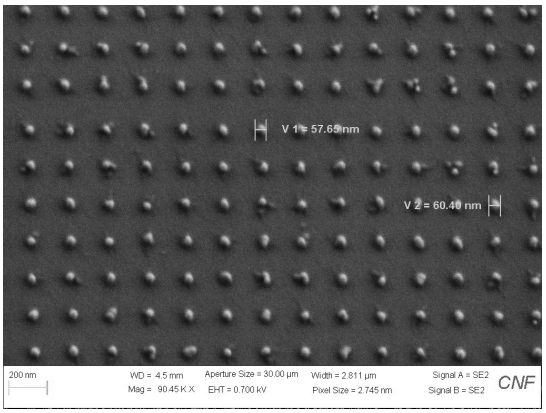

Figure 3: An SEM image of the polymer brushes. The diameter is around 60 nm.

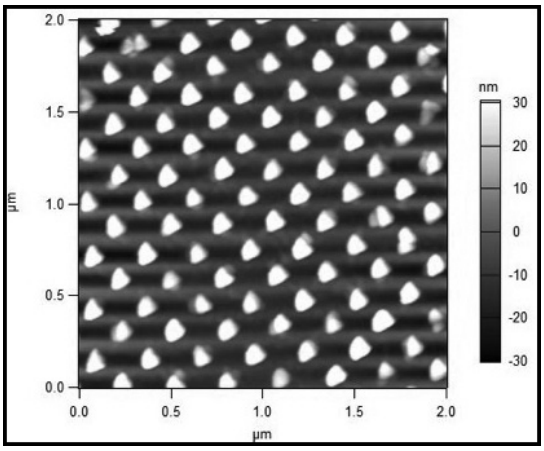

Figure 4: An AFM image of the polymer brushes. The height is around 60 nm.

Engineering Transport in Confined Environments of Stable Radical Polymers

CNF Project Number: 2091-11

Principal Investigator(s): Gregory D. Fuchs

User(s): Albert M. Park

Affiliation(s): Applied Physics, Cornell University

Primary Source(s) of Research Funding: Department of Energy

Contact: gdf9@cornell.edu, amp356@cornell.edu

Primary CNF Tools Used: GCA 5X stepper, wet stations, CVC evaporators, Heidelberg mask writer DWL 2000, DISCO dicing saw

Abstract:

We study properties of a doped radical polymer with a conjugated backbone, which is a promising potential material for an organic radical battery electrode. To compensate the exponential decay of conductivity caused by steric hindrance from covalently attached stable radical, we dope the conjugated backbone using either iodine or 2,3,5,6-tetrafluoro-7,7,8,8-tetracyanoquinodimethane (F4-TCNQ). We characterize the electrical properties as we vary the pendent radical concentration. Transport measurements confirm that doping increases the conductivity by a few to several orders of magnitude, depending on the dopant. Additionally, we use electron paramagnetic resonance (EPR) to investigate the interplay between polarons and stable radical electrons.

Summary of Research:

For enhanced performance of radical polymer based energy storage materials, a high conductivity and a large volume density of electroactive radical electrons are required for efficient current collection and increased capacity, respectively. Our first study in this line of works was to confirm the intrinsic conductivity of poly(2,2,6,6-tetramethyl- piperidenyloxyl-4-yl methacrylate (PTMA), which is one of the model polymers suggested for energy storage [1].

In this work we found that without alternative conduction channels, such as swelling of the polymers with an ionic liquid, the conductivity of non-conjugated radical polymers are closer to that of an insulator than to organic semiconductors. Next, we tried including alternative conductive channels by attaching pendent radical (2,2,6,6-tetramethylpiperidin-1-yl)oxyl (TEMPO) to the conductive conjugated backbone poly(3-hexylthiophene-2,5-diyl) (P3HT) [2].

In this study we were able to achieve increased conductivity, however, we discovered that there is an exponential decrease in conductivity as we increase the number of pendant radicals due to the disorder they create in stacking. In other words, we found a tradeoff between conductivity and the volume density of radical electrons.

As a natural extension to these works, we've focused on doping of the conjugated backbone to increase the conductivity relative to what we found in the intrinsic polymers. In our experiment we chose two dopants: iodine and F4-TCNQ.

The low sublimation point and volatility of iodine allows an easy doping process at room temperature. We were able to see more than five orders of magnitude increase of conductivity for the P3HT control sample that did not have pendent radicals. This trend continued for the polymers with different fractions of pendent radicals showing that the entire curve is shifted upward in conductivity with doping. (Figure 1.) However, iodine also imposes some technical challenges such as dedoping at ambient condition and chemical reaction with metal that composes crucial parts of experimental setup. Thus, while iodine as a dopant for P3HT-TEMPO is very effective at increasing conductivity, at the same time it has limited technical applications due to its volatility and reactivity.

One alternative dopant, which does not suffer from this problem, is F4-TCNQ. When mixed with conjugated backbone polymer in solution state, it is known to form a rigid and semicrystalline charge transfer complex that creates polarons. Due to the rigid formation of a charge transfer complex, it also makes it easier to trace polarons using solution-state EPR.

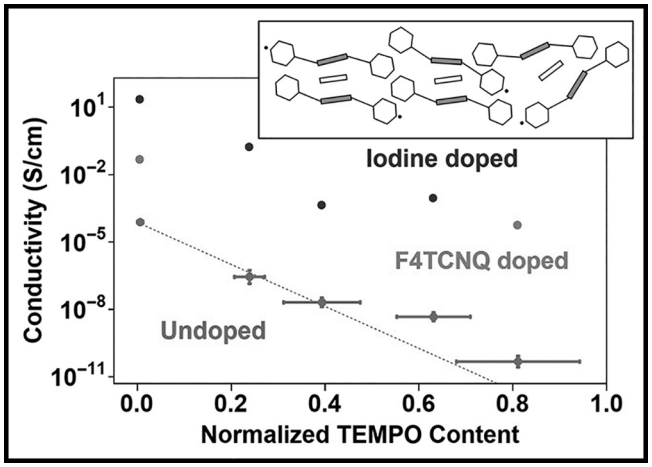

Figure 1: Trend of conductivity as a function of normalized TEMPO content. Blue dots and magenta dots correspond to iodine and F4-TCNQ doped P3HT-TEMPO. Inset shows a schematic of steric hindrance in system of conjugated backbone (orange) with pendent radical (hexagon) in presence of dopants (yellow). (Find full color on pages xiv-xv.)

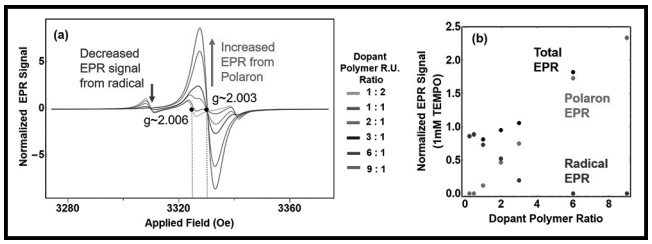

Figure 2: (a) EPR curve of doped conjugated polymer with pendent radical obtained from varying ratio of dopant molecule to polymer repeating unit. (b) Relative contribution of polaron and radical electron to total EPR signal size as a function of dopant polymer ratio. (Find full color on pages xiv-xv.)

In our experiment we've used in-solution doping where we simply mix conjugated polymer and F4-TCNQ in a vial for EPR results. We then cast the dopant on a conjugated polymer film for electrical transport measurement.

The effect of doping of conjugated radical polymer in EPR is clearly visible in Figure 2 (a). In this system, the first source of EPR signal is pendent radicals. Due to hyperfine coupling in the nitroxide radical, we observe a triplet signal when the radicals are isolated from each other. When two or more radical molecules are brought in close distance, exchange coupling become dominant and singlet signal with broader linewidth is observed. Thus, when we vary the percentage of stable radicals that are pendent to the backbone, we get a statistical combination of triplet and singlet. The additional source of EPR signal we introduce from doping of the backbone is polarons. Since polarons are mobile radicals unaffected by hyperfine coupling, they show a singlet lineshape.

These two signals can be distinguished from each other because they have different g-factors and therefore different resonant fields at the same frequency. By fitting the data with known EPR curves for radical electron and polaron, we can quantitatively extract the contribution each component. In Figure 2 (b) we see that the polaron contribution increases linearly with increasing dopant concentration while the radical electron signal decreases. This shows that there is electron transfer between pendent radicals and polarons formed in the backbone.

Finally, with F4-TCNQ doped P3HT-TEMPO we get around 2∼3 orders of magnitude increase in conductivity (Figure 1, magenta points, see page XX for full color). While conductivity increase is not as large as iodine doped case, F4-TCNQ is more stable doping technique, which have negligible dedoping at ambient air and no reaction problem with metal. The consistent trend of decreasing conductivity for higher ratio of pendent stable radical shows that steric hindrance still plays a role in conductivity of thin film doped conjugated polymers (Figure 1, Inset).

References:

[1] Y. Zhang, et al., "Impact of the Synthesis Method on the Solid-State Charge Transport of Radical Polymers." J. Mater. Chem. C 6 (1), 111-118 (2017).

[2] Y. Zhang, et al., "Charge Transport in Conjugated Polymers with Pendent Stable Radical Groups." Chem. Mater. 30 (14), 4799-4807 (2018).

Production of Beta-Tungsten as a Function of Sputtering Pressure

CNF Project Number: 2103-12

Principal Investigator(s): Shefford Baker[1]

User(s): Nathaniel Rogers[2]

Affiliation(s): 1. Department of Materials Science and Engineering,
2. Sibley School of Mechanical and Aerospace Engineering; Cornell University

Primary Source(s) of Research Funding: National Science Foundation Grant DMR 1411024

Contact: shefford.baker@cornell.edu, ngr27@cornell.edu

Website: https://baker.mse.cornell.edu/

Primary CNF Tools Used: MOS hood, AJA sputtering system #2, FleXus film stress measurement system

Abstract:

Metastable phases of tantalum and tungsten that are only present in thin film form are technologically important for the microelectronics industry and show promise for new magnetic memory applications with exhibition of the Giant Spin Hall Effect. Nonetheless, there has been considerable debate about the crystal structural and formation mechanism of these beta phases. Recent advances in the understanding of beta-tantalum provide a road map for how to bring similar clarity to beta-tungsten. A series of five films were made at varying Ag sputter pressures in the CNF AJA #2 sputtering system (3, 5, 6.8, 7, 7.8 mTorr). Substrate curvature was measured before and after each deposition to estimate the average film stress. Theta-2-theta XRD scans were used to examine the resulting crystal structure. Preliminary results show that highly tensile films (made at the higher sputtering pressures) were nearly entirely beta-tungsten, while the other films had significantly more of the alpha phase. While we have conclusively produced beta-tungsten, precise indexing of the theta-2-theta peaks will require higher precision XRD measurements and finder control over film stress generation.

Summary of Research:

This research on tungsten is inspired by recent work our group has done on tantalum [1]. Like tantalum, tungsten can form two phases, either alpha or beta. The alpha phases of both metals have a BCC crystal structure, are present in bulk form, have good electrical conductivity, and are relatively ductile [1]. The beta phases are metastable, found in only some thin films, and are brittle with poor electrical conductivity [2-6]. Both phases of tantalum are technologically important for the microelectronics industry. Additionally, the beta phases of both materials show strong Giant Spin Hall Effect (GSHE), which could be used in advanced magnetic memory devices [5-9]. Yet, even though tantalum has been studied for decades, the formation mechanism and crystal structure for beta-tantalum was only recently well established [1]. Reviewing the literature, it is interesting to note that the historical debates about the formation mechanisms of the metastable beta phases for each material mirror each other closely. Beta-tungsten, like beta-tantalum, for some time was believed to be an oxide rather than a distinct phase [2,6]. At other times, researchers believed that the beta phases of the two metals may share the A15 crystal structure [1,2,6]. In order to sort out the confusion, very carefully controlled deposition experiments need to be performed to understand the role of both sputter pressure and impurity atoms (especially oxygen). Eventually, it was shown that the actual crystal structure of beta-tantalum is a distorted Frank-Kasper sigma structure ($P\bar{4}2_1m$) and requires a template of tungsten oxide to form [1].

Our goal in this research is to explore the formation of beta-tungsten and determine if a similar formation mechanism exists as was discovered for beta-tantalum. The first step in this process is to determine deposition parameters that would reliably produce beta-Tungsten. To do this, the AJA #2 sputtering system was used. Five four-inch wafers were MOS cleaned (but retained the native oxide layer) and sputtered with a 99.995% pure tungsten

target at 450 Watts at argon sputtering pressures of 3, 5, 6.8, 7, and 7.8 mTorr. These pressures were chosen based on the CNF supplied process data that showed that films in this pressure range could be expected to vary their stress widely from highly compressive (3 mTorr) to highly tensile (7 mTorr). Each wafer's curvature was measured with the CNF FleXus stress measurement system immediately before and after deposition to determine the average film stress. The films' thickness was then measured via contact profilometry and it's out-of-plane texture was investigated with XRD theta-2-theta scans to look for the presence of BCC alpha-tungsten or a more complex beta-tungsten crystal structure.

Preliminary results show that the 3 mTorr sample did develop compressive stress with little to no evidence of beta-tungsten. The other films produced high tensile stresses, with the films in the 6.8 to 7.8 mTorr regime possibly being composed almost entirely of the beta phase. It is hard to say with certainty in this preliminary data since the <110> and <220> alpha peaks are nearly identical in location to the <210> and <420> beta peaks which creates some ambiguity. However, we believe that these peaks can be indexed by carefully controlling film stress and shifting them through their stress-free positions. Previous work by Ellis, et al., in 2018 [1] showed that a peak can be unambiguously indexed by tracking its position as film stress changes and noting that it moves through the equilibrium position of a peak corresponding to one phase but not the other.

Future work will include both a sputtering pressure series to first be able to unambiguously index all the observed diffraction peaks, and then an oxygen partial pressure series to determine the amount of oxygen necessary for the formation of beta-tungsten.

References:

[1] Ellis, E. A., et al., Effect of sputter pressure on Ta thin films: Beta phase formation, texture, and stresses. Acta Mater. 150, 317-326 (2018).

[2] Petroff, P., and Reed, W. Resistivity behavior and phase transformations in β-W thin films. Thin Solid Films 21, 73-81 (1974).

[3] Read, M. H., and Altman, C. A new structure in tantalum thin films. Appl. Phys. Lett. 7, 51-52 (1965).

[4] Desai, P. D., et al. Electrical Resistivity of Selected Elements. J. Phys. Chem. Ref. Data 13, 1069-1096 (1984).

[5] Hao, Q., et al. β-tungsten thin films: Structure, electron transport, and giant spin Hall effect. Appl. Phys. Lett. 106 182403 (2015).

[6] Liu, J., and Barmak, K. Topologically close-packed phases: Deposition and formation mechanism of metastable β-W in thin films. Acta Mater. 104 223-227 (2016).

[7] Pai, C.-F., et al. Spin transfer torque devices utilizing the giant spin Hall effect of tungsten. Appl. Phys. Lett. 101 122404 (2012).

[8] Liu, L., et al. Spin-Torque Switching with the Giant Spin Hall Effect of Tantalum. Science. 80, 336 (2012).

[9] Hao, Q., and Xiao, G. Giant Spin Hall Effect and Switching Induced by Spin-Transfer Torque in a W / Co 40 Fe 40 B 20 / MgO Structure with Perpendicular Magnetic Anisotropy. Phys. Rev. Appl. 3 34009 (2015).

Nanotube Transistor Arrays on a TEM Substrate

CNF Project Number(s): 2486-16, 2719-18

Principal Investigator(s): Jonathan S. Alden, Paul L. McEuen

User(s): Jonathan S. Alden, Joshua S. Alden

Affiliation(s): Esper Biosciences Inc; Department of Physics, Cornell University

Primary Source(s) of Research Funding: National Institutes of Health, National Science Foundation

Contact: jonathan.alden@gmail.com, mceuen@ccmr.cornell.edu, ja698@cornell.edu

Primary CNF Tools Used: Low pressure chemical vapor deposition (LPCVD) furnaces (oxide, nitride), Autostep i-line stepper, ABM contact aligner, SC4500 evaporators, Oxford 80 RIE

Abstract:

We use photolithography to fabricate nanotube transistor devices on substrates with thin nitride windows, which can be imaged using transmission electron microscopy (TEM). Our device architecture permits us to characterize a given nanotube both electrically, and by high-resolution TEM. In low-dimensional systems, such as nanotubes, where nanoscale surface and defect structure can have profound influences on the electrical properties, we expect this combined nanoscale imaging and electrical characterization to yield insights that will inform the design of nanoscale sensors.

Summary of Research:

The study of low-dimensional materials, such as carbon nanotubes, graphene, and molybdenum disulfide, has been an area of growing interest over the past decades, in part due to their promise as molecular sensors. Due to their one-to-few-atom thickness, the properties of such materials often depend sensitively on surface adsorbates, substrate-surface interaction and defect structure.

Improving sample cleanliness, for example, enabled the first observations of spin-orbit coupling in carbon nanotubes [1] and, more recently, the fractal quantum Hall effect, known as Hofstadter's butterfly, in graphene [2]. In order to understand these nanoscale structures and subsequently design improved sensors, a device architecture is needed which combines the atomic-level characterization afforded by TEM with the electronics characterization ability enabled by a gated, transistor-like geometry.

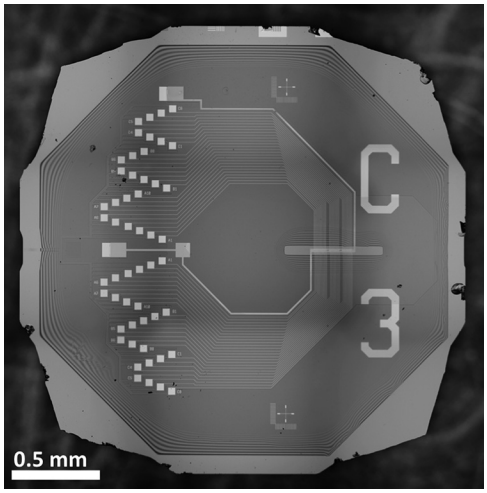

Figure 1: Optical image of microfabricated TEM grid with 26 pairs of source-drain electrodes, a top gate, and a thin nitride window for TEM imaging after top-gate is removed via chemical etching.

We demonstrate that we can produce arrays of gated nanotube sensors devices, with reasonably high yield that can be characterized afterwards by TEM. Our design also keeps parasitic capacitance from our electrodes to the highly resistive silicon substrate low enough to enable electronic measurements of our transistors at MHz bandwidth.

We fabricate nanotube devices on TEM grids using a combination of photolithography and standard nanotube growth and transfer techniques [3]. Figure 1 shows one of such devices, having 26 source-drain electrode pairs and two top gates. Between a few of the electrode pairs are individual nanotubes, which have been transferred prior to the deposition of a gate dielectric, and top-gate. The device fabrication involves using nine masks to define the various structures, which have been designed to yield nanotube devices with good gating characteristics, as well as low capacitive coupling between nearby electrodes.

The outline of the fabrication procedure is as follows. We begin by using low pressure chemical vapor deposition (LPCVD) to deposit the low-stress nitride on a 300 μm-thick silicon substrate, which will ultimately become our TEM window. We later deposit electrodes, and use backside alignment followed by reactive ion etching

(RIE) to expose rectangles on the back of the wafer, which will later be used for a potassium hydroxide (KOH) through-etch. Arrays of parallel nanotubes are grown by CVD on a separate quartz substrate, coated with poly(methyl methacrylate) (PMMA), lifted off with KOH, and transferred onto the device substrate [3], where unwanted areas are patterned and etched using RIE. We use atomic layer deposition (ALD) to deposit a gate dielectric, after which we pattern and evaporate a gold top-gate. The surface is then coated with a KOH protection layer, and the devices are placed in hot KOH, which etches the silicon exposed on the back, to both release individual grids and to etch the silicon away from behind the nitride window. Later, the nanotube devices will be imaged through this window using TEM. The protection layer is then removed, and the grids are cleaned with oxygen plasma. Our fabrication process typically yields at least one electrically-connected, gated nanotube on 75% of the TEM grids.

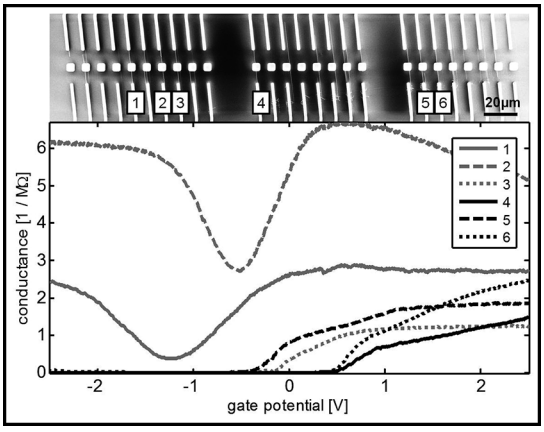

Figure 2: Upper: Scanning electron microscope image of nanotubes between source-drain electrodes, passing over thin nitride windows. Lower: Corresponding conductance measurements as a function of top gate voltage showing six conducting nanotubes with varying characteristics.

Figure 2 shows an SEM image of nanotubes patterned between the source-drain electrode pairs, imaged prior to top-gate deposition. The squares in the center are thin nitride windows for low-background TEM imaging. After completion of the device fabrication, these nanotubes are characterized electrically, shown in the lower portion of Figure 2. All of these nanotubes can be gated to have resistance lower than 1 MΩ (50 kΩ/μm) showing that they have a low defect density, and good coupling to the top gate. Nanotubes 1 and 2 can be seen to be metallic, while nanotubes 3-6 are semiconducting.

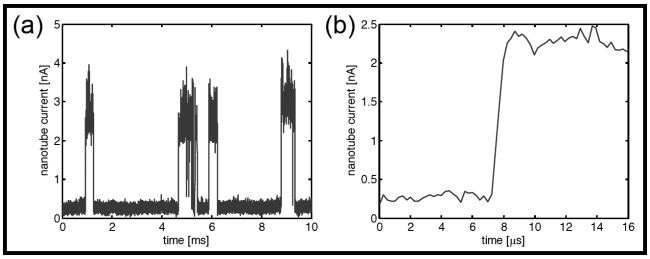

Figure 3: High-speed measurement of nanotube random telegraph signal showing (a) fluctuations in nanotube current and (b) measured rise time of less than 1 μs.

Furthermore, we can probe the electrical characteristics at high speeds in the MHz range. Previous research has shown that single charge fluctuations in a dielectric can be detected by semiconducting carbon nanotubes as random telegraph signals [4]. As show in Figure 3, our devices are also capable of measuring such signals, but at higher speeds with rise times less than 1 μs.

After characterizing the nanotubes electronically, we can etch away the gold top-gate, and image them by TEM to determine, for example, the nanotube diameter. Figure 3 shows one such nanotube, which can be seen to be single-walled (single dark lines running parallel to the arrows), and 4 nm in diameter (the width between those lines).

In principle, our fabrication procedure can be applied to many different CVD-grown low-dimensional materials with only minor modifications, and may lead to the development of improved nanoscale sensors capable of high-speed molecular sensing.

References:

[1] F. Kuemmeth, et al., Nature 452 448-452 (2008).

[2] C. R. Dean, et al., Nature 497, 598-602 (2013).

[3] L. Jiao, et al., J. Am. Chem. Soc. 130, 12612-12613 (2008).

[4] T. Sharf, et al., Nano Lett. 14 (9) 4925-4930 (2014).

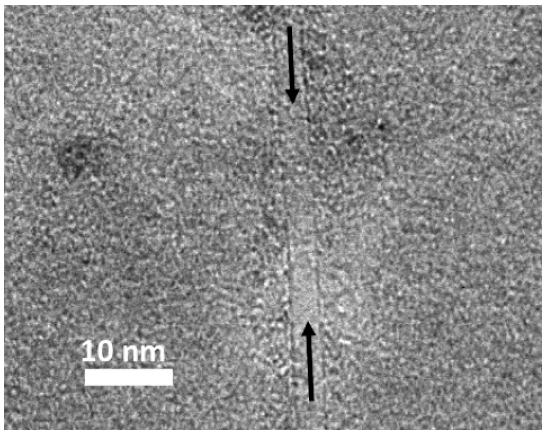

Figure 4: TEM image of a nanotube imaged through a thin nitride window, after top-gate removal.

Inertial Spreading and Imbibition of a Liquid Drop Through a Porous Surface

CNF Project Number: 2565-17

CNF Principal Investigator(s): Michel Louge

User(s): Shilpa Sahoo

Affiliation(s): Mechanical and Aerospace Engineering, Cornell University

Primary Source(s) of Research Funding: NSF-CBET-1637531

Contact: michel.louge@cornell.edu, ss3624@cornell.edu

Primary CNF Tools Used: Goniometer and the availability of other wonderful tools at CNF

Summary of Research:

The project that has been be accomplished in Cornell NanoScale Science and Technology Facility (CNF) is a part of the ISS imbibition project with NASA. The ISS project requires capillary plates with hydrophilic coatings.

To get a hydrophilic surface, the capillary plates need to be coated with SAM coating. For feasible and strength purposes, the capillary plates must be made of metal. The plate must first be coated with a thin layer of gold after the metal plate has been machined to the required roughness. Because SAM is stable on gold but rarely on other metals, gold plating must first be applied.

All the gold coated plates were then coated with self-assembled-monolayer (SAM) coatings in Professor Susan Daniel's Lab (https://chemistry.cornell.edu/susan-daniel).

Thiols 6-Mercapto-1-Hexanol, 6-Mercaptohexanoic Acid 90% and 8-Mercaptooctanoic Acid 95% were used. The contact angles were measured in CNF's Rame 500 Goniometer to record the resulting contact angles and their hysteresis. Corresponding hydrophilic angles of 26°, 46°, and 68° were obtained for 6-Mercapto-1-Hexanol, 6-Mercaptohexanoic Acid 90% and 8-Mercaptooctanoic Acid 95% respectively.

Fabrication of Graphene-Encapsulated Photocathodes

CNF Project Number: 2584-17
Principal Investigator(s): Melissa A. Hines
User(s): William J.I. DeBenedetti

Affiliation(s): Chemistry and Chemical Biology, Cornell University
Primary Source(s) of Research Funding: Center for Bright Beams, a NSF-funded Science and Technology Center (STC)
Contact: melissa.hines@cornell.edu, wjd74@cornell.edu
Primary CNF Tools Used: SC4500 odd-hour evaporator

Abstract:

A new technique for the fabrication of graphene-encapsulated photocathodes is being developed. The monolayer-thick graphene film will protect the photocathode from oxidation by residual gases or the atmosphere while having only a small effect on the intensity and brightness of the generated electron beam.

Summary of Research:

Photocathodes are materials that eject electrons under illumination. By their very nature, high-performance photocathodes must be made from materials that lose electrons easily — in other words, materials that are easily oxidized. For example, many photocathodes are either coated with alkali metals (e.g., Cs/GaAs) or comprised of alkali metals (e.g., Cs_3Sb). This presents a technical challenge, as exposure to even trace amounts of O_2 or H_2O will destroy or degrade the photocathode. For highest performance, the photocathodes must also be atomically flat and extremely homogeneous.

To meet these challenges, we are developing a technique to produce a graphene-encapsulated photocathodes. The key challenge in this project is ensuring that every step of the fabrication leaves no residue on the surface, as even monolayer levels of contamination could significantly reduce photoelectron transmission and beam brightness.

In the first step of fabrication, commercial graphene monolayers, which are grown on a copper foil, are coated with a thin gold layer in the SC4500 evaporator. The copper foil is then removed with an aqueous etchant, allowing the graphene side of the gold-coated graphene to be adhered to a low energy substrate. The gold film is then removed by a second aqueous etch. As shown in Figure 1, we have successfully transferred intact, single-layer-thick graphene films to cm-size substrates as confirmed by both optical microscopy and Raman analysis. The near-atomic cleanliness of the transferred films has been quantified using photoelectron spectroscopy.

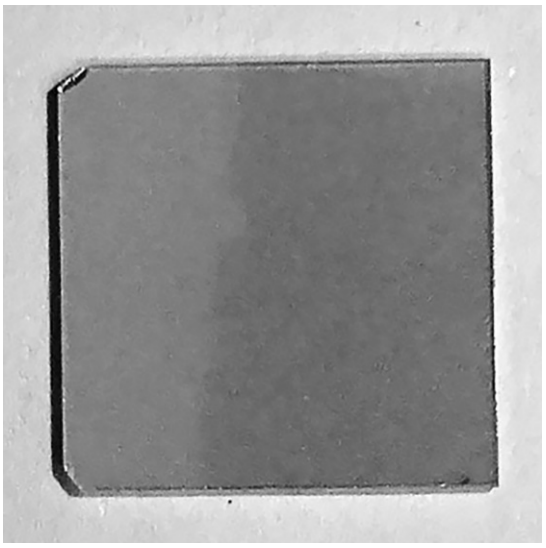

Figure 1: Optical image of a transparent substrate with a graphene monolayer deposited on the right half of the substrate. The graphene monolayer causes a small decrease in the transmission of visible light.

Al_2O_3 Deposition and Characterization on III-Nitride Surfaces for Improvement of Dielectric/Semiconductor Interface Properties and Device Reliability

CNF Project Number: 2684-18

Principal Investigator(s): Fatemeh Shahedipour-Sandvik

User(s): Benjamin McEwen

Affiliation(s): Colleges of Nanoscale Science and Engineering, SUNY Polytechnic Institute

Primary Source(s) of Research Funding: Army Research Laboratory

Contact: sshahedipour-sandvik@sunypoly.edu, bmcewen@sunypoly.edu

Primary CNF Tools Used: Oxford FlexAL ALD, Woollam spectroscopic ellipsometer

Abstract:

We investigate the use of atomic layer deposition (ALD) to deposit Al_2O_3 and the effect of a post deposition forming gas anneal on the structural properties of the dielectric. Scanning transmission electron microscopy (STEM) and energy dispersive x-ray spectroscopy (EDS) indicate that after low temperature (350°C) anneal in forming gas, the oxide bulk structure and interface do not undergo significant change.

Summary of Research:

Gallium nitride (GaN) is considered as an excellent candidate for the high voltage device platform because of its superior material properties. It has the potential for lower power losses, higher efficiency, and smaller system volume and weight [1,2]. The next generation of reliable and enhancement mode AlGaN/GaN based high electron mobility transistors (HEMTs) requires further development of high quality passivation and gate dielectric materials. Passivation dielectric is used to reduce current collapse, and gate dielectric is used to reduce gate-leakage current. However, the introduction of a dielectric layer leads to issues associated with the dielectric/(Al)GaN interface trap states, bulk trap states within the dielectric, and surface defect states. Device properties depend on the dielectric used and the density of these interface, bulk, and surface states associated with the dielectric. Decreasing the density of these trap states is essential for good device quality.

Unintentionally doped (UID) GaN was grown on c-plane sapphire using metal-organic chemical vapor deposition (MOCVD). 20 nm of Al_2O_3 was deposited using the Oxford FlexAL ALD system at CNF. Trimethylaluminum (TMA) was used as the aluminum precursor and water as the oxidant; the substrate was maintained at 300°C during the deposition. After the oxide deposition, the thickness of the layer was confirmed using the Woollam spectroscopic ellipsometer at CNF. A piece of the wafer was then cleaved off and subjected to annealing in forming gas (95% N_2/ 5% H_2) ambient at 350°C for 10 minutes.

Lamellae were cut from the as-deposited Al_2O_3-on-GaN and the annealed Al_2O_3-on-GaN samples using focused ion beam (FIB). STEM imaging and EDS mapping were used to evaluate structural evolution in the Al_2O_3, especially at the interface with GaN, as a result of the anneal. Figure 1 shows a high angle annular dark field (HAADF) image of the as-deposited Al_2O_3. As expected, the interface between the Al_2O_3 and GaN is abrupt since the ALD process is surface reaction limited and no additional processes were performed after the deposition. Figure 2 shows a HAADF image of the annealed sample. Additionally, Figures 3a and 3b show the EDS mapping of aluminum and oxygen, respectively in the annealed sample.

From these images, it can be concluded that at moderate temperatures of 350°C or less, the structure of the Al_2O_3/ GaN interface is stable, and minimal interdiffusion between the dielectric and semiconductor are observed.

Additionally, metal-insulator-semiconductor (MIS) capacitors were fabricated. Capacitance-voltage (C-V) characteristics were measured to evaluate the effects of forming gas anneal on the electrical properties of the dielectric/semiconductor interface. Both frequency dispersion and C-V hysteresis were reduced in the sample that underwent the anneal, compared to the as-deposited sample, indicating that the density of interface states was reduced as a result of the forming gas anneal.

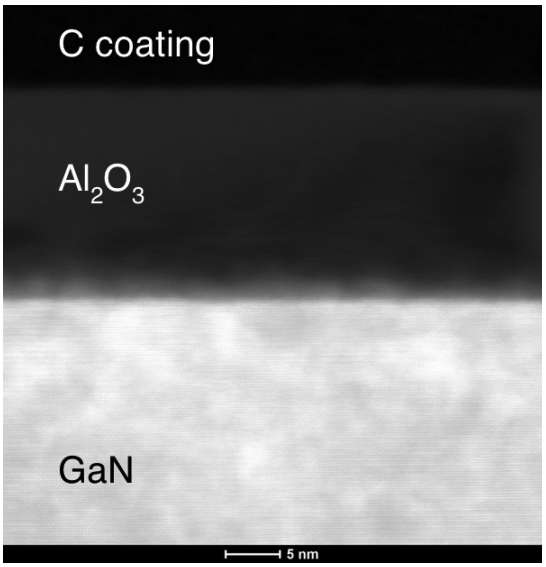

Figure 1: HAADF image of as-deposited Al_2O_3-on-GaN. The apparent thickness of the interface is most likely due to roughness of the surface of the GaN.

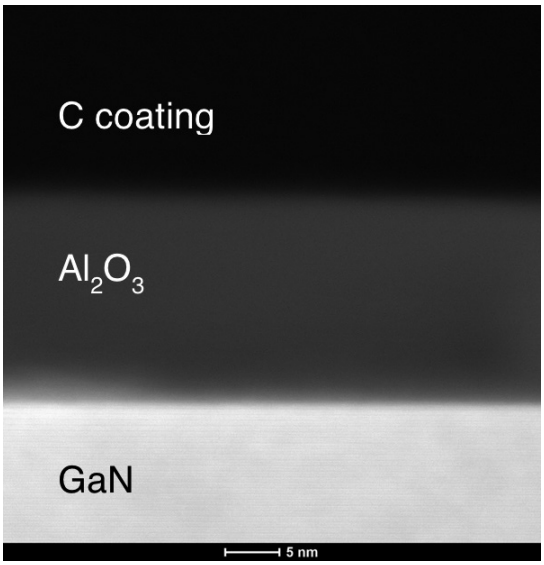

Figure 2: HAADF image of Al_2O_3-on-GaN subjected to annealing in forming gas at 350°C for 10 min.

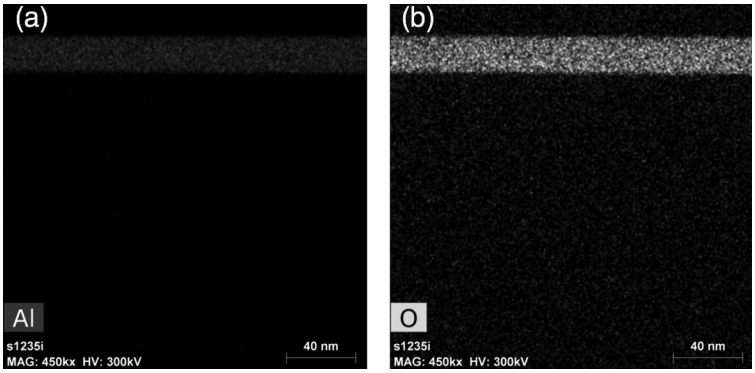

Figure 3: (a) EDS map of Al and (b) EDS map of O from Al_2O_3-on-GaN subjected to annealing in forming gas at 350°C for 10 min. The Al and O are segregated to the oxide layer and no interdiffusion between the Al_2O_3 and GaN is observed. (Find full color on pages xiv-xv.)

References:

[1] K. Shenai, R. S. Scott and B. J. Baliga, "Optimum Semiconductors for High-Power Electronics," Transactions on Electron Devices, vol. 36, no. 9, pp. 1811-1823, 1989.

[2] M. Bhatnagar and B. J. Baliga, "Comparison of 6H-SiC, 3C-SiC, and Si for power devices," Transactions on Electron Devices, vol. 40, no. 3, pp. 645-655, 1993.

Thermal and Electrical Properties of Quasi-1D van der Waals Nanowires

CNF Project Number: 2698-18

Principal Investigator(s): Deyu Li

User(s): Yang Zhao, Lin Yang

Affiliation(s): Department of Mechanical Engineering, Vanderbilt University

Primary Source(s) of Research Funding: National Science Foundation

Contact: deyu.li@vanderbilt.edu, yang.zhao@vanderbilt.edu, lin.yang@vanderbilt.edu

Primary CNF Tools Used: Heidelberg mask writer DWL2000, Autostep i-line stepper, LPCVD Nitride - B4, GSI PECVD, AJA sputter deposition, AJA ion mill

Abstract:

Using the CNF cleanroom, we have successfully fabricated microdevices for nanowire electrical and thermal conductivity measurements. These microdevices allow for experimental studies of the transport properties of various types of van der Waals nanowires, including $NbSe_3$ and Ta_2NiSe_5. Interesting observations such as record long ballistic phonon transport in $NbSe_3$ nanowires have been obtained. Systematic studies are being conducted to understand the underlying physical mechanisms.

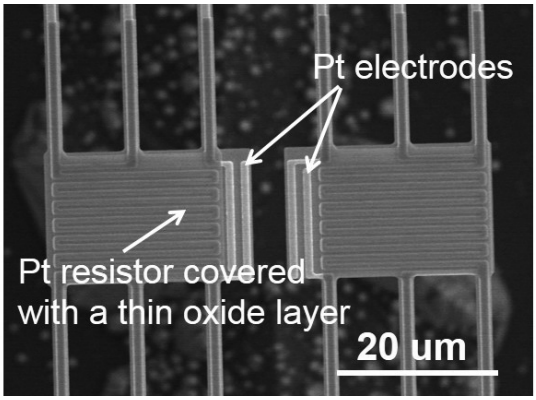

Figure 1: A scanning electron microscopy (SEM) image of the microdevice consisting of two suspended membranes integrated with serpentine Pt coils as both resistance heaters and thermometers for transport property measurements of individual nanowires.

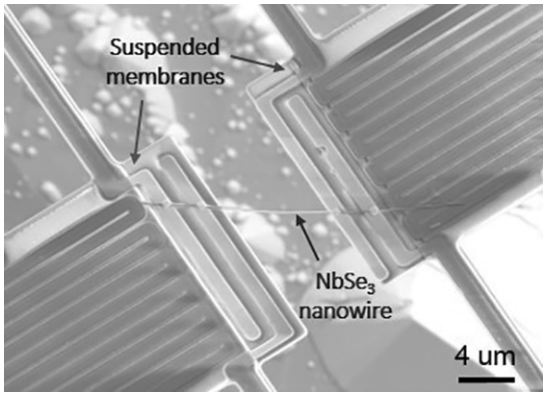

Figure 2:An SEM micrograph of an individual 135 nm-diameter $NbSe_3$ nanowire placed between the two suspended membranes.

Summary of Research:

Two Ph.D. students, Yang Zhao and Lin Yang have been trained and used CNF cleanroom facilities to fabricate microdevices as shown in Figure 1. The microdevice consists of two side-by-side suspended SiN_x membranes integrated with serpentine Pt coils serving as both resistance heaters and thermometers. Yang Zhao made three trips to CNF and spend a total of about five weeks to fabricate the devices while Lin Yang only joined the first trip and spent about ten days at CNF.

The nanofabrication process involves LPCVD SiN_x film growth, sputtering deposition of Pt films, PECVD SiO_2 film deposition, photolithography and etching, and the students have got extensive experience of using various nanofabrication tools to prepare the microdevices. In about half year time frame, the students have successfully fabricated a few wafers of devices, which have been used to measure the electrical and thermal conductivities of $NbSe_3$ and Ta_2NiSe_5 nanowires.

To measure the electrical and thermal properties of nanowires, individual nanowire samples are placed to bridge the two suspended membranes as shown in Figure 2. The device is then put into a cryostat for electrical and thermal transport measurements, during which one suspended membrane is heated up by resistance Joule heating and a portion of the heat is transferred to the other suspended membrane. Through monitoring the resistance change of the Pt coils, the temperature of both membranes can be simultaneously obtained. This allows for extraction of the thermal conductivity of the nanowire. In addition, the four extra Pt electrodes at the inside of the two membranes allow for four-point measurements of the nanowire electrical conductivity.

Our group has used this approach to conduct extensive measurements of various nanowires, nanotubes and nanoribbons. To date, the newly fabricated microdevices have been adopted to study thermal properties of two kinds of van der Waals nanowires made of $NbSe_3$ and Ta_2NiSe_5. van der Waals nanowires are a class of materials composed of covalently bonded molecular chains assembled together via weak van der Waals interactions, which renders interesting electrical and thermal transport properties as demonstrated by some of our recent studies [1,2].

For example, the measured thermal conductivity of a 135 nm-diameter $NbSe_3$ nanowire is displayed in Figure 3 together with the contributions from both electron and phonon as energy carriers. $NbSe_3$ nanowires demonstrate two spontaneous charge density waves (CDW) as the temperature drops to 145 K and 59 K, respectively, which correspond to condensation of a large portion of free electrons and lead to variations in their electrical conductivity and electron contribution to the thermal conductivity. The unusual peaks in the lattice thermal conductivity are attributed to electron-phonon scattering, which provide direct and unambiguous evidence for the importance of electron-phonon scattering in lattice thermal transport, which has been lacking so far. In addition, we have used the newly fabricated devices to probe ballistic transport of phonons in $NbSe_3$ nanowires and observed record long ballistic transport distance and currently we are probing the underlying physical mechanisms for this unexpected ballistic phonon transport.

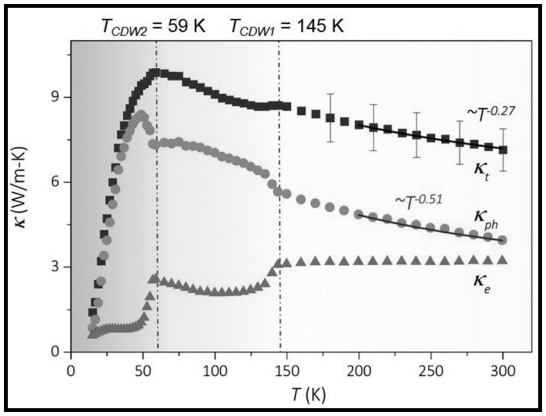

Figure 3: Distinct signatures of electron-phonon scattering in the lattice thermal conductivity of a 135 nm-diameter $NbSe_3$ nanowire in the temperature range of 15-300 K. The electron and phonon contributions are labelled as κ_e and κ_{ph}, respectively, and the total thermal conductivity is denoted as κ_t.

References:

[1] Q. Zhang, C. Liu, X. Liu, J. Liu, Z. Cui, Y. Zhang, L. Yang, Y. Zhao, T. T. Xu, Y. Chen, J. Wei, Z. Mao, and D. Li, "Thermal Transport in Quasi-1D van der Waals Crystal $Ta_2Pd_3Se_8$ Nanowires: Size and Length Dependence," ACS Nano 12, 2634-2642 (2018).

[2] L. Yang, Y. Tao, J. Liu, C. Liu, Q. Zhang, M. Akter, Y. Zhao, T. T. Xu, Y. Xu, Z. Mao, Y. Chen, and D. Li, "Distinct Signatures of Electron-Phonon Coupling Observed in the Lattice Thermal Conductivity of $NbSe_3$ Nanowires," Nano Lett. 19, 415-421 (2019).

Fabricating Lithographically Designed Cylindrical Colloidal Particles

CNF Project Number: 2704-18

Principal Investigator(s): Prof. Fernando Escobedo

User(s): Prajwal Bangalore Prakash

Affiliation(s): Chemical and Biomolecular Engineering, Cornell University

Primary Source(s) of Research Funding: Escobedo Funding

Contact: fe13@cornell.edu, pb526@cornell.edu

Primary CNF Tools Used: Spinners and hot plates in Class-II resist room, AutoStep i-line stepper

Abstract:

Materials with characteristic structural features on the colloidal scale (10 nm to 10 μm) are potentially important for applications in electronics, optics, high density memory, microelectromechanical machines, and tissue engineering. In this project, we are exploring our understanding to allow for rational design of desired materials from colloidal building blocks. For this purpose, we have exploited a class of colloidal particles formed by photolithography in a polymeric photoresist (SU-8) [1-3]. The objective of the current project is to study the equilibrium assembled structures formed by the cylindrical colloidal particles under confinement. These structures are predicted using Monte Carlo simulation model; and we are now focusing on validating the assembly behavior using experiments.

Summary of Research:

Our first step was to fabricate micron-sized monodisperse cylindrical particles using the photolithography technique. We used the epoxy-based negative photoresist, SU-8 2001 and adopted the following procedure to achieve the target dimension [2]:

(1) Spin coating of the SU-8 2001 photoresist on top of a sacrificial layer (OmniCoat™) on a silicon substrate achieving the desired average height of 0.98 μm. For a 0.98 μm layer, SU-8 can be spun at 500 rpm for 10s, immediately followed by a step at 3000 rpm for 30s.

(2) Exposure of the wafer through a Cr photomask with round holes using a 5X stepper (GCA Autostep i-line). The average diameter of the particle (~1.605 μm) is controlled by exposing the resist to the ultraviolet light (365 nm) through a photomask with rounded holes with a focus value of -1.4 μm and exposure time = 0.22s.

(3) Post-exposure bake of the SU-8 layer: the wafer was placed on a vacuum hotplate at 65°C for 1 min and 95°C for 2 min to crosslink the exposed photoresist. The wafer was allowed to cool to ambient temperature before proceeding to the next step. Next, the wafer is then placed in ~ 100 mL of SU-8 developer for 1 min and then rinsed with IPA.

(4) The particles are then released by using Remover PG and sonication in an ultrasonic cleaner.

Before placing the particles in the buffered solutions of surfactants, a sample of particles in DI water was redeposited on a silicon wafer and imaged by SEM (Zeiss Supra 55VP or Zeiss Ultra 55). The average and standard deviation of the heights and diameters of the particles were measured on the images (Figure. 2). We estimated about 6.3% and 4.7% polydispersity in height and diameter, respectively. We note in Figure 1 that the two ends of the cylinders were not identical: one end had sharp edges that were globally flat (although not smooth); the other end had more rounded edges (arrow). The flat end was the one that was in contact with the OmniCoat sacrificial layer. We obtained the size distributions by analysis of scanning electron micrographs. The fabricated SU-8 particles are then dispersed in water and Tergitol NP70 surfactant solvent medium.

References:

[1] Badaire, Stéphane, Cécile Cottin-Bizonne, and Abraham D. Stroock. "Experimental investigation of selective colloidal interactions controlled by shape, surface roughness, and steric layers." Langmuir 24.20 (2008): 11451-11463.

[2] Badaire, Stéphane, et al. "Shape selectivity in the assembly of lithographically designed colloidal particles." Journal of the American Chemical Society 129.1 (2007): 40-41.

[3] Hernandez, Carlos J., and Thomas G. Mason. "Colloidal alphabet soup: Monodisperse dispersions of shape-designed lithoparticles." The Journal of Physical Chemistry C 111.12 (2007): 4477-4480.

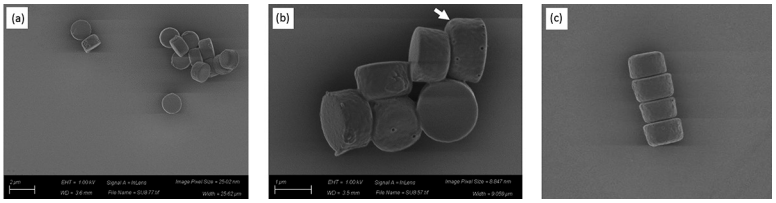

Figure 1: (a)-(c) Structure of the SU-8 particles obtained using scanning electron micrographs. Arrow (white) shows the curvature of edge of one of the particles. (c) The column arrangement of the particles shows variation in particle diameter.

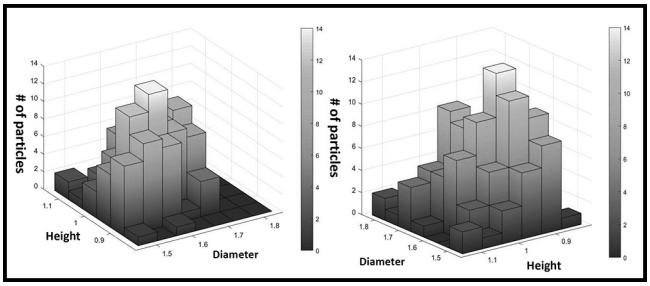

Figure 2: Histogram of height and diameter of the particles. The statistics is taken for ~ 200 particles diameter and height data. The skewness in diameter is about 0.056 in diameter and 0.305 in height. This indicates an approximate symmetric distribution in the profile.

Development of Microsensors for Air Quality Monitoring

CNF Project Number: 2728-18

Principal Investigator(s): Alex Deyhim

User(s): Nicole Chu, Jin Luo, Chuan-Jian Zhong, Shanana Yan

Affiliation(s): Materials Science and Engineering, Cornell University

Primary Source(s) of Research Funding: MEng Materials Science and Engineering FlexSurfaces/CCMR Jumpstart

Contact: akd9@cornell.edu, nc537@cornell.edu

Primary CNF Tools Used: Metal film deposition, photolithography, mask making equipment, optical pattern generator, ABM contact aligner, wafer processors

Abstract:

Air pollution is a major problem that is dangerous not only to the environment but to the health and safety of humans. Due to the increase in air pollution in recent years there has in turn been a decline in health. Particularly conditions such as respiratory and cardiovascular diseases have seen a rise in prevalence. People who had preexisting conditions have seen their conditions worsen due to this rise and there has been a rise in prevalence of health defects such as headaches, dizziness, trouble breathing, damage to the liver and in some cases cancer. As such there is a need for a device to monitor air pollution levels for personalized use. Existing technology lacks sensitivity and selectivity as well as cost efficiency and are not equip for personalized use. Gold nanoparticles fabricated into microelectrode array devices allow for the selectivity and sensitivity need to make theses sensors. Working with company FlexSurfaces and the Cornell NanoScale Science and Technology Facility, we have used the clean room facilities to begin developing the technology for low-cost sensors with high sensitivity for use in portable and wearable air quality monitoring systems.

Summary of Research:

The design of the sensors is very important. The parameters and shape of the microelectrode used in the array impacts its performance when measuring air quality. The composition of the nanostructure thin film also has a large impact on the performance of the sensor to detect VOCs. Current array measurements are made of combinations of the following, finger width (FW, 5 µm, 10 µm), finger space (FS, 5 µm, 10 µm), and finger length (FL, 100 µm, 200 µm). Previously gathered sensor array response data shows that smaller parameter values for width, length and space typically result in a higher response sensitivity when tested and exposed to various VOCs. (See Figure 1.)

Flexible devices use a similar mask design and parameters as the glass substrates. (See Figure 2.) The material used in the flexible design is Kapton also known as polyimide. This material is both flexible and inexpensive making it perfect for this application. This design while testing and optimized for glass array devices still needs alterations to maximize ability on flexible substrates. This is currently being tested and studied.

The photos in Figure 3 demonstrate the diminished finger space as seen in the first photo the finger space is so small you cannot see it and in the second is disappearing. The final photo shows what a well-made finger space should look like. This problem with the disappearing and diminishing of the devices parameters was predicted to be one of two problems — over exposure or loose contact. Several experiments were carried out to find a solution to these problems.

The possible problem of a loose contact was addressed by cleaning the mask more thoroughly before contact with the substrate. While the problem of overexposure was delft with in a more expansive method.

Design #	FS (µm)	FW (µm)	FL (µm)
1	10 (1)	10 (1)	100 (-1)
2	10 (1)	5 (-1)	200 (1)
3	5 (-1)	10 (1)	200 (1)
4	5 (-1)	5 (-1)	100 (-1)

Design	*W*/µm	*S*/µm	*L*/µm
1	5	5	100
2	5	10	100
3	10	5	100
4	10	5	300
5	10	10	100
6	10	10	400

Figure 1: Device parameters for glass samples (right) and polyimide samples (left).

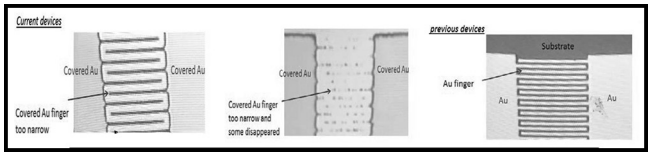

Figure 3: The finger spaces between first devices and older devices. As can be seen in the photos on the left, the finger space has been diminished.

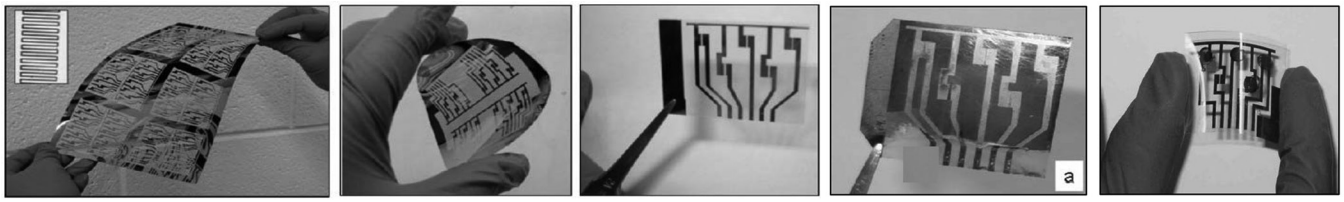

Figure 2: Examples of flexible devices. Devices are very versatile as demonstrated in the photographs.

In order to address overexposure a single substrate was taken and exposed at six different exposure times. Exposure times from 4-11 seconds were tested. The image below shows an example of what one of these test samples would look like. One can see in the images the finger of a sample produced at six seconds, nine seconds and eleven seconds. From these images one can already see how the finger parameters are affected by the exposure time. The sample at eleven seconds has a much smaller finger space than the sample at six seconds. After etching and careful observations under the microscope it could be seen that six seconds was the exposure time that developed the optimal device parameters for flexible substrates. All future tests were carried out with flexible substrates at six seconds exposure times.

Testing of the array devices is done at Binghamton University. Where further processing of the wafers is first conducted. The interdigitated microelectrode devices are first coated with a sensing tin film which is prepared by molecularly-mediated assembly of nanoparticles. Samples were then housed in Teflon® chambers and hooked to computer-interfaced multimeters, resistance was measured. Vapor sources and N_2 were connected via tubing. Vapor concentration in ppm moles per liter was calculated from partial vapor pressure. N_2 is used as the reference gas, and all experiments were performed at room temperature, 22 ± 1°C.

The graphs in Figure 4 are examples of glass and polyimide device response profiles to benzene and or hexane. The images show that both the glass and flexible devices show somewhat similar response profiles. This means that only slight adjustments will need to be made to the device parameters in order to maximize their ability on the polyimide substrate.

Conclusions:

Through this project we have developed a process for fabricating interdigitated microelectrodes on flexible polyimide substrates. This development process differed from the one used on glass substrates in order to ensure the optimal parameters. Particularly within the process the exposure time needed adjustments for flexible substrates. Tests conducted so far have shown that the microfabricated IMEs on both glass and polyimide substrates worked well, showing similar response profiles to certain VOC's.

Further testing is still being carried out to evaluate the performance of these sensors. Experiments into other possible substrates such as paper are being considered. A systematic study is underway to evaluate the device parameters. As we gather more information, we are beginning to develop a prototype sensor device to be used in air quality monitoring.

References:

[1] Wang L, et al. Sensing Arrays Constructed from Nanoparticle Thin Films and Interdigitated Microelectrodes. Sensors (Basel). 2006;6(6):667-679. Published 2006 Jun 22.

[2] Craft, Elena. "Microsensors Help Map Crowdsourced Pollution Data." GreenBiz, GreenBiz Group Inc., 26 June 2013, www.greenbiz.com/blog/2013/06/26/microsensing-measure-air-pollution-palm-your-hand.

[3] "A Brief Guide to Atmospheric Pollutants." Compound Interest, Compound Interest, 8 May 2015, www.compoundchem.com/2015/05/05/atmospheric-pollutants/.

[4] Knox, A., et al. "Air Pollution Air Pollution Monitoring Air Pollution Monitoring and Sustainability Air Pollution Sustainability." Encyclopedia of Sustainability Science and Technology, 2012, pp. 167-203., doi:10.1007/978-1-4419-0851-3_373.

[5] "Air Conditions", Bloomberg Pursuits, April 15, 2019.

[6] "Indoor Air Quality." EPA, Environmental Protection Agency, 16 July 2018.

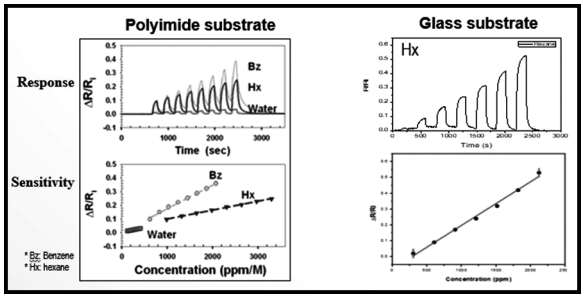

Figure 4: Response profiles for polyimide (left) and glass (right) substrates to hexane and for poluimide benzene vapors.

Scissionable Polymer Photoresist for Extreme Ultraviolet Lithography

CNF Project Number: 2751-18

Principal Investigator(s): Christopher Kemper Ober

User(s): Abhaiguru Ravirajan

Affiliation(s): Materials Science and Engineering, Cornell University

Primary Source(s) of Research Funding: INTEL Corporation

Contact: christoper.ober@cornell.edu, ar2362@cornell.edu

Primary CNF Tools Used: ASML 300C DUV stepper, ABM contact aligner, JEOL-9500 e-beam lithography, P10 profilometer

Abstract:

Researchers across the globe are intensively working on photoresists that can show high resolution down below 10 nm in a single-step process. Extreme ultraviolet (EUV) and electron-beam (e-beam) lithography are the most prominent candidates to create such small structures in resists. The difficulty in achieving such small feature size arises due to the RLS tradeoff, where the resists must simultaneously satisfy the resolution, line width roughness and sensitivity requirements. Also, another major concern with EUVL is the problem of stochastics due to lesser number of photons. Through our work, we believe that chemically amplified photoresists based on scissionable polymers are potential candidates to overcome these challenges. Our work focuses on polyaldehydes based low ceiling temperature (T_c) polymers that unzip upon exposure to DUV (deep ultraviolet)/EUV light sources due to main chain cleavage of the polymer backbones. So far, we have synthesized polyphthalaldehyde (PPA) based photoresists and studied their performances with the incorporation of various photoacid generators (PAGs) and base quencher.

Summary of Research:

One of the limitations with EUV light source is that there are much less photons available for the photochemical reactions of the photoresists. Either low or uneven light radiation energy across the exposed region can cause random defects during the lithography processes. Thus, it is desirable to pursue multimechanism photoresists that involves intrinsically depolymerizable polymers and the concept of chemical amplification. This approach shares some feature of the scissionable photoresist using main chain cleavage, but in contrast makes effective use of limited light exposure through the chain depolymerization of the resist polymer. The chain scissionable polymers usually have low ceiling temperatures (T_c) and contain weak chemical bonds, which can be cleaved by external triggers and thus starting the depolymerization process [1]. Due to their interesting properties, they have been widely utilized as sacrificial components in many areas, such as resist imaging, fabrication of porous materials, and transient electronics.

In our study, we focus on the synthesis of one kind of chain scissionable polymers, polyphthalaldehydes, via metal-free anionic polymerization of aldehyde monomers that are promoted by superbases bases with alcohol initiators [2]. Not only can this method produce linear PPA with tunable molecular weights and low dispersity, but also provides the possibility to introduce extra functional groups at the chain ends. Later, the PAGs can be introduced into the side chains using highly efficient post-polymerization reactions [3].

Materials and Methods; Synthesis:

Photoresist solution containing 5 wt.% PPA in cyclohexanone blended with common ionic and nonionic PAG's, for example, triphenylsulfonium triflate was prepared in varying ratios of 2-10 wt.% to PPA. Further base quenchers were introduced to these PPA-PAG blends [4]. The solution was then spin coated onto a silicon wafer at 3000 rpm for 1 min and post apply baked at 90°C for 1 min to remove excess solvent.

Results and Discussions:

The PAG blended polymer solution was exposed to 254 nm mid-UV radiation through a mask containing

patterns using ABM contact aligner. The pattern on the exposed resist was then directly observed through Nikon Microscope Cameras in CNF without the use of any developer or post-exposure processing techniques at different times after exposure. As shown in Figure 1, the image pattern continued to develop gradually over time. This is mainly because of the vaporization of monomers due to the main chain depolymerization under mid-UV radiations. Further the resist solution containing PAG, Base quencher blend was exposed to mid-UV radiations. As seen in Figure 2, good quality pattern was observed compared to the PAG only blended polymer patterns and the self-development of pattern was found to be more controlled.

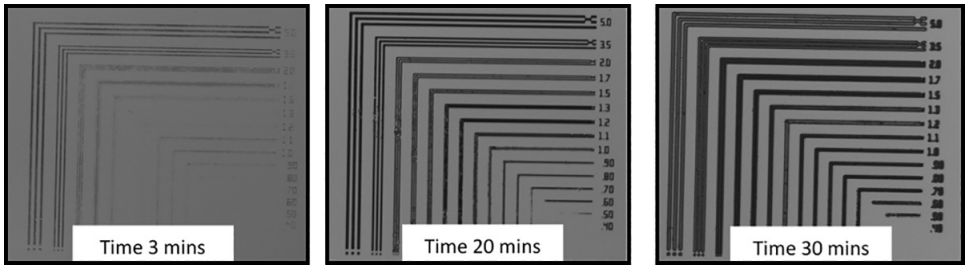

Figure 1: Optical microscope images of PAG blended PPA resist observed at different times after exposure to 1 mJ/cm² mid-UV radiation using ABM contact aligner.

Similar performance of these photoresists was also observed when exposed to 248 nm DUV radiation using ASML 300C DUV stepper. Well-defined 1:1-line spaced positive tone patterns were observed for an exposure dosage in the range of 1-4 mJ/cm² without any use of post-exposure. Further, these resists were evaluated under e-beam lithography using CNF JEOL 9500 Lithography tool. While large amounts of residues can be easily found at exposed areas, good 1:1 line patterns with feature sizes from 1000-400 nm were obtained for exposure dosage in the range of 75-100 μC/cm² by atomic force microscopy (AFM), as shown in Figure 3.

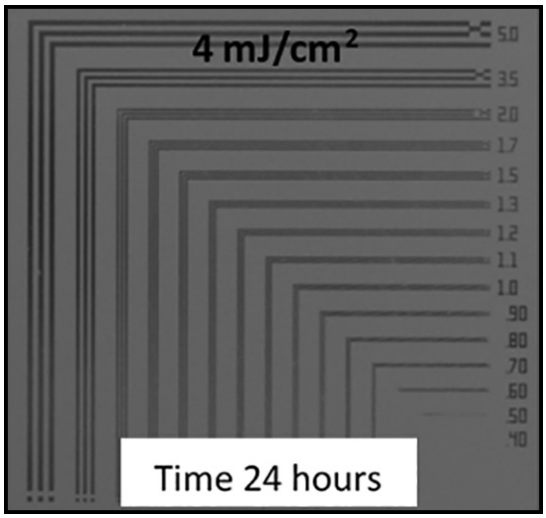

Figure 2: Optical microscope image of PAG, base quencher blended PPA resist observed at 24 hours after exposure to mid-UV radiation showing enhanced image quality.

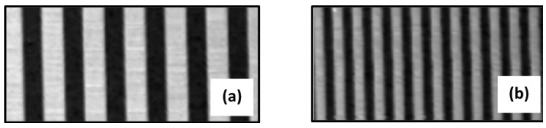

Figure 3: 1:1-line space patterns with feature size: (a) 600 nm (b) 400 nm observed under AFM after exposure to 75 μC/cm² e-beam radiation.

Summary:

In summary, photocleavable polymer photoresists show promising results when introduced to mid-UV, DUV and e-beam lithography. By introducing an optimized percentage of PAG and base quencher into resist solution, high contrast patterns under extremely low exposure dosages can be achieved. With these preliminary findings, PAG functionalized derivatives of PPA will be introduced to lithography, and the performances will be evaluated for achieving improved resolution and LER.

References:

[1] Sasaki, T., et al., Photoinduced depolymerization in poly(olefin sulfone) films comprised of volatile monomers doped with a photobase generator. Journal of Polymer Science Part A: Polymer Chemistry, 2012. 50(8): p. 1462-1468.

[2] Wang, F. and C.E. Diesendruck, Polyphthalaldehyde: Synthesis, Derivatives, and Applications. Macromol Rapid Commun, 2018. 39(2).

[3] Hernandez, H.L., et al., Triggered transience of metastable poly(phthalaldehyde) for transient electronics. Adv Mater, 2014. 26(45): p. 7637-42.

[4] Natsuda, K., et al., Study of Acid-Base Equilibrium in Chemically Amplified Resist. Japanese Journal of Applied Physics, 2007. 46(11): p. 7285-7289.

Quantum Materials for Communication, Computing, and Storage

CNF Project Number: 2801-19

Principal Investigator(s): Debdeep Jena, Huili Grace Xing

User(s): John Wright, Phillip Dang, Zexuan Zang, Jashan Singhal, Hyunjea Lee

Affiliation(s): 1. Materials Science and Engineering, 2. Applied and Engineering Physics, 3. Electrical and Computer Engineering; Cornell University

Primary Source(s) of Research Funding: ONR-DJ

Contact: djena@cornell.edu, grace.xing@cornell.edu, jgw92@cornell.edu, pd382@cornell.edu, zz523@cornell.edu, js3452@cornell.edu, hl2255@cornell.edu

Primary CNF Tools Used: Autostep 2000 I-Line stepper, JEOL 6300, AJA sputter, Vecco AFM, DISCO dicing saw

Abstract:

The integration of new material properties into electronics devices creates new possibilities for device performance, architecture, and function. We therefore investigate the fabrication and applications of materials with exceptional properties, including superconductivity, ferromagnetism, ferroelectricity, and topologically non-trivial electronic states.

Summary of Research:

Two-dimensional (2D) materials, which allow the extreme scaling down of transistors with their atomically thin structure, are a promising candidate for the next generation electronics. One of the challenges for these applications is complementary metal oxide semiconductor (CMOS) devices. For CMOS, there should be a complementary pair of n-type and p-type field effect transistors (FETs) whose mobility and threshold voltage are well matched. There have been many studies about n-type 2D materials that make n-type field effect transistors (FETs), but p-type 2D materials with sizable band gap have not been well explored. For a pMOS option, we have investigated tungsten diselenide (WSe_2). WSe_2 is a good candidate for CMOS applications since it shows ambipolar behavior as well as relatively high hole mobility. We have been making p-type FETs using exfoliated WSe_2 flakes. The Autostep stepper is used to make the substrate for 2D material transfer, the JEOL 6300 is used to define patterns for metal contacts, and the AJA sputtering system is used to deposit metals. The I-V characteristics of representative device is shown in Figure 1(a) and 1(b). Maximum drive current reaches more than 20 μA/μm, the on/off current ratio is more than seven decades, and the upper bound of contact resistance is around 75 kΩ·μm, which is comparable to some of the best results in literature [1].

Spin-orbit torque (SOT) is a physical phenomenon where a material with large spin-orbit coupling can exert a torque on the magnetic moment of an adjacent ferromagnet (FM). This effect is applicable to magnetic memory, where information can be stored in the magnetization direction of the FM, and SOT can be used to control that magnetization direction. The efficiency of magnetic manipulation by SOT is dependent on the types of materials used and the quality of the interface between them. Topological insulators (TI) are a class of materials with strong spin-orbit coupling, an inversion of the band structure, and surface states where the spin and momentum of electrons are interdependent. These attributes can lead to more efficient SOTs and make FM/TI bilayers very promising for magnetic memory devices [1]. However, in many reports, at least one material of the FM/TI bilayer is sputtered [1-3]. To further enhance the performance of FM/TI bilayer, we grow FM/TI structures using molecular beam epitaxy (MBE) in one shot without exposure to air. Here, we report our advances in the MBE growth and characterization of TIs and FMs bilayers that are applicable to SOT devices.

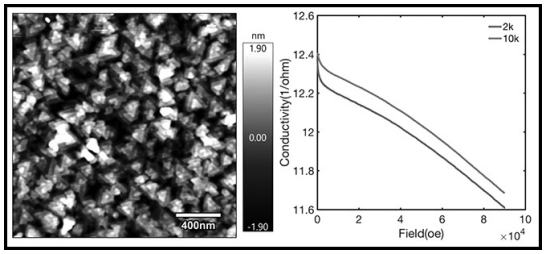

Figure 1: AFM surface height map of Bi_2Se_3 grown on GaAs, showing < 1 nm RMS roughness (left) and magnetoresistance of Bi_2Se_3 grown on GaAs (right).

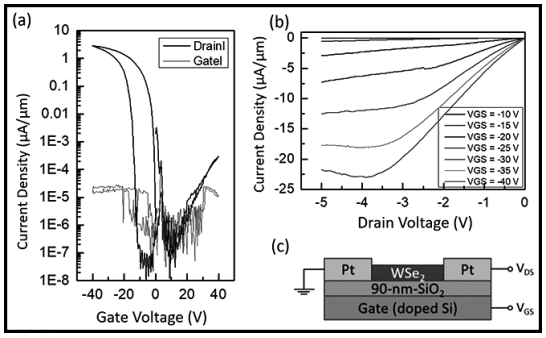

Figure 2: (a) Transfer curve of WSe_2 pFET, (b) Output curve of WSe_2 pFET, and (c) Cross-sectional image of WSe_2 pFET.

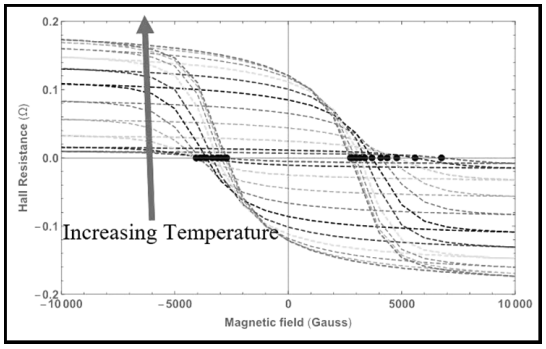

Figure 3: Temperature-dependent AHE measurement from 10K - 300K for Mn_4N film on MgO (001). The saturation Hall resistance increases with temperature. (Find full color on pages xiv-xv.)

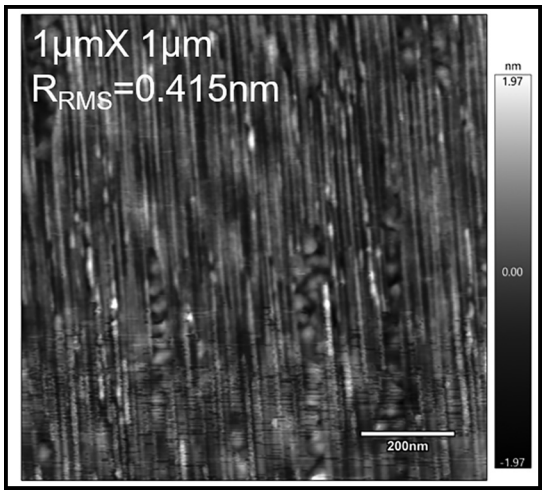

Figure 4: AFM surface height map of NbN/AlN/NbN heterostructure grown on 6H-SiC by MBE.

Recently, room temperature switching of the magnetization of a FM using Bi_2Se_3 as the TI have been reported [2,3], revealing the merits of using Bi_2Se_3 in FM/TI structures. We are now optimizing growth condition of Bi_2Se_3 on different substrates including GaAs and sapphire. Thanks to the weak VdW interaction between Bi_2Se_3 and substrates, high quality single crystal Bi_2Se_3 have been successfully grown on both substrates with smooth surface (RMS < 1 nm), as shown in the atomic force microscopy (AFM) image shown in Figure 1. However, it is found that bulk states exhibit metallic electrical transport characteristics, as shown by the temperature-dependent resistance in Figure 2. Topological insulators should be insulating in the bulk, so the metallic behavior indicates that the Fermi level is not in the bulk band gap of Bi_2Se_3. Tuning the Fermi level into the bulk bandgap of Bi_2Se_3 by electrostatic gating or doping the film could also lead to higher SOT efficiency.

For the ferromagnetic layer in our FM/TI structure, we are exploring Mn_4N, one of the few known magnetic nitride materials. We are optimizing the MBE growth of Mn_4N on various substrates such as MgO, STO and GaN. Through measurement techniques such as vibrating sample magnetometry and anomalous Hall effect (AHE) measurements, we have confirmed perpendicular magnetization and low saturation magnetization which are both beneficial for magnetic memory device applications. To make our samples suitable for these measurements, we use the dicing saw and metal deposition systems such as the CHA thermal evaporator. The shape of the AHE signal, as shown in Figure 3, nearly forms a parallelogram and is indicative of perpendicular magnetic anisotropy, which is desirable for higher-density magnetic memory.

The phenomena of superconductivity and the integration of superconducting materials with normal state materials are utilized in applications such as quantum computing and single flux quantum computing. We investigate the possibility of realizing epitaxial integration of III-N semiconductors with metallic superconducting materials such as NbN through the growth of thin film heterostructures by molecular beam epitaxy. We have demonstrate that epitaxial NbN/AlN/NbN heterostructures can be grown on 6H-SiC substrate with RMS roughness less 0.5 nm. Measurements to observe the Josephson effect in these structures are ongoing.

References:

[1] H. C. P. Movva et al., ACS Nano 9, 10402-10410 (2015).

[2] Mellnik, A. R., et al. "Spin-transfer torque generated by a topological insulator." Nature, 511(7510), 449-451 (2014).

[3] Han, Jiahao, et al. "Room-temperature spin-orbit torque switching induced by a topological insulator." Physical review letters 119.7 (2017): 077702.

[4] Mahendra, D. C., et al. "Room-temperature high spin-orbit torque due to quantum confinement in sputtered BixSe1-xfilms." Nature materials 17.9 (2018): 800.